ON THE DYNAMICS OF EARTH-ORBITING FLEXIBLE SATELLITES WITH MULTIBODY COMPONENTS

by

L. Vu Quoc and J. C. Simo

Memorandum No. UCB/ERL M86/29

1 April 1986

ON THE DYNAMICS OF EARTH-ORBITING FLEXIBLE SATELLITES WITH MULTIBODY COMPONENTS

by

L. Vu-Quoc and J. C. Simo

Memorandum No. UCB/ERL M86/29

1 April 1986

ELECTRONICS RESEARCH LABORATORY

College of Engineering
University of California, Berkeley
94720

TITLE PAGE

ON THE DYNAMICS OF EARTH-ORBITING FLEXIBLE SATELLITES WITH MULTIBODY COMPONENTS

by

L. Vu-Quoc and J. C. Simo

Memorandum No. UCB/ERL M86/29

1 April 1986

ELECTRONICS RESEARCH LABORATORY

College of Engineering
University of California, Berkeley
94720

On the Dynamics of Earth-Orbiting Flexible Satellites with Multibody Components

L. VU-QUOC
Structural Engineering and Structural Mechanics Division,
University of California, Berkeley, CA 94720.

J.C. SIMO
Applied Mechanics Division,
Stanford University, Stanford, CA 94305.

Table of Contents

March 8, 1986

On the Dynamics of Earth-Orbiting Flexible Satellites with Multibody Components

L. VU-QUOC
Structural Engineering and Structural Mechanics Division,
University of California, Berkeley, CA 94720.

J.C. SIMO
Applied Mechanics Division,
Stanford University, Stanford, CA 94305.

Abstract

We propose in this paper a novel treatment to the dynamics of satellites with flexible multibody components. Our formulation makes essential use of the property of invariance under superposed rigid body motion of fully nonlinear structural theories. This property enables us to refer the dynamics of the satellite directly to the inertial frame. In addition, geometric instability effects are automatically accounted for in the formulation. To avoid numerical ill-conditioning, the dynamics of the far field and of the near field are treated separately by introducing a floating frame which is a parallel translate to the inertial frame with origin placed at the center of mass of the satellite. Constraint conditions that are typically used in standard treatments to determine the orientation of the floating frame are thus entirely by-passed. The proposed formulation can accommodate an unrestricted class of maneuvers under the action of follower actuator forces and gravity force, and is particularly well suited for the dynamics of flexible multibody systems undergoing a broad range of structural deformations.

1. Introduction

The configuration of earth-orbiting satellites has evolved markedly from rigid vehicles (spinners, dual spinners), hybrid rigid-elastic systems (dual spinners with flexible appendages), towards future generation of flexible large space structures (space antennae, solar power satellites); see Kline [1979]. The size of space antennae may vary from 50 to 300 meters, to even one kilometer in diameter. The projected solar power satellite, for instance, measures 5 kilometers in width by 10 kilometers in length. Spacecrafts of this size, constructed using light weight materials, are therefore highly flexible.

Satellite dynamics: Floating frames. Current approaches to the dynamics of flexible structures in orbit are largely based on the assumption of small deformation, and rely on the use of a floating reference frame to describe the structural displacements. To prevent rigid body motions relative to the floating frame, one imposes constraints on the displacement field of the entire body. There are typically five types of floating reference frame: (1) locally attached frame, (2) principal axis frame, (3) Tisserand frame, (4) Buckens frame, and (5) rigid body mode frame (Canavin & Likins [1977]). When the structure has a central rigid body with flexible appendages around, the frame is attached to the rigid body (the locally attached frame) and no constraint equation is needed. For structures with distributed flexibility, other types of floating frame should be

used. In these frames, the origin is fixed at the center of mass of the deformed structure, i.e., one seeks to annihilate the linear momentum relative to the floating frame. Its orientation is then defined by adding constraints concerning the relative angular momentum. When small structural deformation is assumed, the Buckens frame is the most widely used since one can either use the free-free elastic modes to eliminate these (holonomic) constraints from the equations of motion (Canavin & Likins [1977]), or apply the Gram-Schmidt orthogonalization procedure on an independent basis functions to eliminate the Buckens constraints (Benson & Hallquist [1985]).

For the type of highly flexible large space structures described above there is no guarantee that deformations remain small. Hence, traditional approaches employing the small strain assumption would yield only a first order approximation. In addition, for fast rotating flexible structures, linearized theories can yield grossly inaccurate results, Simo & Vu-Quoc [1986c]. Our methodology, on the other hand, represents a departure from traditional approaches in that, by employing fully properly invariant nonlinear structural theories, the dynamics of the structure is directly referred to the inertial frame; thus completely by-passed the need for a floating reference frame. Clearly, proper invariance with respect to superposed rigid body motions is a property that plays a essential role. Within the proposed framework, the inertia term of the translation part becomes linear, simply mass times acceleration, whereas the inertia term associated with the rotation part has identical structure as in the equations of motion of a rigid body (Simo & Vu-Quoc [1985,86a]).

Theoretically, we have presented in Simo & Vu-Quoc [1985-86a] equations of motion that completely describe the dynamics of a free-free fully nonlinear beam subject to three-dimensional large overall motions, together with detailed numerical treatment. For flexible satellites, however, since structural deformations are extremely small compared to the distance separating the center of the earth and the satellite, numerical ill-condition would result if the dynamics of the satellite were referred directly to an inertial frame. We propose to avoid this numerical ill-conditioning simply by expressing the dynamics of flexible satellites relative to a parallel translate of the inertial frame, with origin at the center of mass of the satellite. The procedure to integrate the resulting equations of motion are discussed in detail. Further, the action of configuration dependent actuator control forces can be conveniently accounted for in the formulation (Simo & Vu-Quoc [1986a-b]).

Multibody dynamics. Satellite configurations with modules of different degrees of flexibility furnish an example of an important class of flexible multibody systems. A robot manipulator arm consisting of human-like links connected by joints is another example of a multibody system. Today's commercial robots

are often designed to be rigid because of the limitation of currently available analytical tools — mainly in the active control of these mechanical systems (Dubowsky [1985]).

There exists a vast body of literature on multibody dynamics starting with the pioneering work by Hooker & Margulies [1965] and Roberson & Wittenburg [1967]. Although most of the research in this area is focused on systems of rigid bodies, recently, attention has been directed to the study of flexible multibody systems. An overview of several approaches to the dynamics of n-body systems can be found in Jerkovsky [1977]. An extensive reference list is contained in Huston [1981]. Ho & Herber [1985] classifies multibody systems into several categories in the order of increasing difficulty in the formulation as follows: (1) two-rigid-body system, (2) all-rigid topological tree multibody system,† (3) cluster of flexible appendages around a central rigid body, (4) topological tree multibody system with rigid interconnected bodies and flexible terminal bodies, (5) all-flexible chain system, and (6) all-flexible topological tree multibody system. Treatment of the flexible chain system (5) may be found for example in Hughes [1979] with some restriction in the speed of motion of the angles at the joints, while treatment of the more complex topological tree multibody system is explored in Huston [1981]. In general, with the presence of closed-loops, additional non-holonomic constraints have to be included in the equations of motion (e.g., Kane & Levinson [1983]), and thus require special care in the numerical integration procedure.

It is emphasized that as a direct by-product of our formulation, one can easily analyze flexible multibody configurations of classes (5) and (6) of the Ho-Herber classification, and even with the presence of closed loops. This is achieved without alteration of the formulation and without any additional constraints since hinge conditions are accounted for in a straightforward manner using the spatial Galerkin finite element discretization of the equations of motion. In Simo & Vu-Quoc [1985], we presented several examples that involve flexible chains undergoing large overall motions. Further, owing to the full nonlinearity of our formulation, should the chain be made more flexible, large deformations in these links would be obtained. Also, no limitation on the speed of evolution of the system is imposed. We shall illustrate this feature by an example of a flexible closed-loop chain subjected to large overall motions and undergoing large deformation.

Although the proposed methodology is applicable to a large class of structural elements, — rods, plates, shells, 3-D continua — we shall limit our

† That is a set of $(n+1)$ bodies interconnected by n points, each of which is common to two bodies. The tree topology thus implies the absence of closed loops.

discussion to the case of a flexible satellites composed of beam elements. An outline of the paper is as follows. In Section 2, we summarize the fully nonlinear theory of rod formulated in Simo [1985], and introduce some notation that will be extensively used in the paper. In section 3 attention is focussed on the dynamics of flexible satellites: the decomposition of the deformation map into the far field and the near field, the concept of rotationally-fixed floating frame, and loading conditions of particular interest in satellite application. Computational procedures to treat the coupled far-field/near-field dynamics are addressed in Section 4. Finally, numerical examples are given in Section 5.

2. A finite-strain rod model: Summary and notation

Kinematic description. (See Figure 3.1)

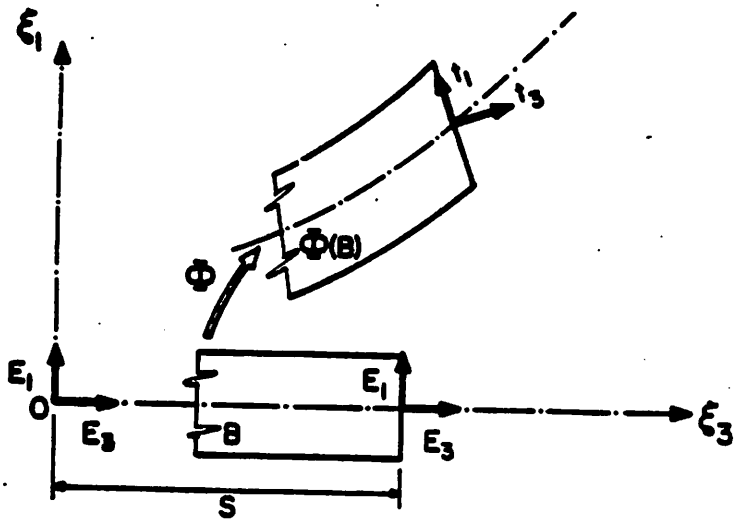

Figure 2.1. *Kinematic description of the rod. Material frame* $\{\mathbf{E}_1, \mathbf{E}_2, \mathbf{E}_3\}$ *and cross-section frame* $\{\mathbf{e}_1, \mathbf{e}_2, \mathbf{e}_3\}$.

Consider a (fixed) material orthonormal reference frame $\{O;\mathbf{E}_1, \mathbf{E}_2, \mathbf{E}_3\}$, with base point $O \in \mathbf{R}^3$ and associated Cartesian coordinate system (X_1, X_2, S). A beam of length L and cross section $\Omega \subset \mathbf{R}^2$ occupies the domain $B := \Omega \times [0, L] \subset \mathbf{R}^3$ in its undeformed (reference) configuration. For simplicity, we assume that the beam is prismatic, initially straight, such that the point O is the centroid of the cross section at $S = 0$; $(\mathbf{E}_1, \mathbf{E}_2)$ coincide with the principal axes of inertia of the cross section. Let $\{O;\mathbf{e}_1, \mathbf{e}_2, \mathbf{e}_3\}$ denote the inertial frame such that $\mathbf{e}_k \equiv \mathbf{E}_k$, for k=1,2,3. Consider the deformation map $\phi: B \to \mathbf{R}^3$ which maps a point $X \in B$ with coordinates (X_1, X_2, S) into a point $x = \phi(X) \in \mathbf{R}^3$. Let X_o

denote a material point on the undeformed centroidal line with coordinates $(0, 0, S)$ and x_o its image by ϕ.

Let $\{\mathbf{t}_I(S,t)\}_{\{I=1,2,3\}}$ represent the orthonormal basis vector of a moving frame attached to a typical cross section with $t \in \mathbf{R}_+$ being a time parameter. The origin of the moving frame is fixed at the centroid x_o of the cross-section. The basis vector $\mathbf{t}_3$ remains normal to the section at all times. Further, initially at $t = 0$, let $\mathbf{t}_I(S,0) \equiv \mathbf{E}_I$ for $I = 1,2,3$. The basic kinematic assumption is based on the following relation for the position vector of x, denoted by $\mathbf{x}$,

$$\mathbf{x} = \mathbf{x}_o + X_I \mathbf{t}_I \dagger \tag{2.1a}$$

with $\mathbf{x}_o$ denotes the position vector of point x_o. Let us introduce the map $\phi_o : [0, L] \to \mathbf{R}^3$ and the orthogonal transformation map $\mathbf{A}: \mathbf{R}^3 \to \mathbf{R}^3$ with the following definition. A material frame $\{X_o; \mathbf{E}_1, \mathbf{E}_2, \mathbf{E}_3\}$ is mapped into the frame $\{x_o; \mathbf{t}_1, \mathbf{t}_2, \mathbf{t}_3\}$ such that

$$\mathbf{x}_o := \boldsymbol{\phi}_o(S,t) = \phi_{oi}(S,t)\, \mathbf{e}_i\,, \tag{2.1b}$$

$$\mathbf{t}_I(S,t) = \mathbf{A}(S,t)\, \mathbf{E}_I = \Lambda_{iI}(S,t)\, \mathbf{e}_i\,, \quad (I = 1,2,3)\,, \tag{2.1c}$$

where Λ_{iI} are components of $\mathbf{A}$ viewed as a two-point tensor

$$\mathbf{A}(S,t) = \Lambda_{iI}(S,t)\, \mathbf{e}_i \otimes \mathbf{E}_I\,. \tag{2.1d}$$

Accordingly, any possible configurations of the rod is defined by a map $S \in [0, L] \to \boldsymbol{\phi}(S) := (\boldsymbol{\phi}_o(S), \mathbf{A}(S))$. Before summarizing the formulation of our rod model, we introduce some notation that will be extensively used in what follows.

Notation. Recall that physically, each orthogonal transformation $\mathbf{A}$ defines a *finite rotation* about the eigenvector $\boldsymbol{\theta}$ associated the only real eigenvalue 1 : $\mathbf{A}\,\boldsymbol{\theta} = \boldsymbol{\theta}$ — the trivial case where $\mathbf{A} = \mathbf{1}_3$, the identity, is excluded. The magnitude of the rotation angle is $\|\boldsymbol{\theta}\|$. $\mathbf{A}$ can be parametrized either in terms of Euler angles or in terms of quaternion parameters. In what follows, we shall often use the notation $\mathbf{1}_k := Diag[1,...,1]$ to denote the unit matrix in $\mathbf{R}^{k \times k}$.

A skew-symmetric matrix has either a single eigenvalue equal to zero or all three eigenvalues each equal to zero. Eliminating the trivial case where all three eigenvalues are zero (the zero rotation), physically any skew-symmetric matrix $\overset{\vee}{\boldsymbol{\theta}}$ represents an *infinitesimal rotation* about the eigenvector $\boldsymbol{\theta} \in \mathbf{R}^3$ associated with the only zero eigenvalue such that $\overset{\vee}{\boldsymbol{\theta}}\,\boldsymbol{\theta} = \mathbf{0}$. In coordinates, relative to a basis $\{\mathbf{e}_i\}$ in $\mathbf{R}^3$, we have $\overset{\vee}{\boldsymbol{\theta}} = \overset{\vee}{\theta}_{ij}\, \mathbf{e}_i \otimes \mathbf{e}_j$ and $\boldsymbol{\theta} = \theta_i\, \mathbf{e}_i$ such that

$$[\overset{\vee}{\theta}_{ij}] = \begin{bmatrix} 0 & -\theta_3 & \theta_2 \\ \theta_3 & 0 & -\theta_3 \\ -\theta_2 & \theta_1 & 0 \end{bmatrix}, \quad \{\theta_i\} = \begin{Bmatrix} \theta_1 \\ \theta_2 \\ \theta_3 \end{Bmatrix} \tag{2.2}$$

† Summation convention on repeated indices is implied.

Further, in relation with the cross product, we recall that $\overset{\vee}{\boldsymbol{\theta}}\,\mathbf{h} = \boldsymbol{\theta} \times \mathbf{h}$, for any $\mathbf{h} \in \mathbb{R}^3$. We shall often use the notation $[\boldsymbol{\theta} \times] \equiv \overset{\vee}{\boldsymbol{\theta}}$ where $\boldsymbol{\theta} \in \mathbb{R}^3$ is called the *axial vector* of the skew-symmetric matrix $\overset{\vee}{\boldsymbol{\theta}}$.

Finally, infinitesimal rotations are *linearized* finite rotations about the identity. We recall that given $\mathbf{A}$ orthogonal, there exists a skew-symmetric matrix $\overset{\vee}{\boldsymbol{\theta}}$ such that $\mathbf{A} = \exp[\overset{\vee}{\boldsymbol{\theta}}]$. One has the following explicit formula (e.g., Argyris [1982])

$$\exp\,[\overset{\vee}{\boldsymbol{\theta}}] = \mathbf{1}_3 + \frac{\sin\,\|\boldsymbol{\theta}\|}{\|\boldsymbol{\theta}\|}\,\overset{\vee}{\boldsymbol{\theta}} + \frac{1}{2}\,\frac{\sin^2\,(\|\boldsymbol{\theta}\|/2)}{(\|\boldsymbol{\theta}\|/2)^2}\,\overset{\vee}{\boldsymbol{\theta}}{}^2 \tag{2.3}$$

which, in vector form, is often credited to Rodrigues (Goldstein [1980], p. 165).

Partial differential equations of motion. The local form of the equations governing the dynamics of our rod model is summarized in BOX 1 below

BOX 1. *Partial differential equations of motion.*

$$\frac{\partial \mathbf{A}(S,t)}{\partial S} = \overset{\vee}{\boldsymbol{\omega}}(S,t)\,\mathbf{A}(S,t)\,, \qquad \frac{\partial \mathbf{A}(S,t)}{\partial t} = \overset{\vee}{\mathbf{w}}(S,t)\,\mathbf{A}(S,t)$$

$$\boldsymbol{\Gamma} = \mathbf{A}^T \frac{\partial \boldsymbol{\phi}_o(S,t)}{\partial S} - \mathbf{E}_3\,, \qquad \boldsymbol{\Omega} = \mathbf{A}^T\,\boldsymbol{\omega}$$

$$\mathbf{n} = \mathbf{A}\,\frac{\partial \psi(S,\boldsymbol{\Gamma},\boldsymbol{\Omega})}{\partial \boldsymbol{\Gamma}}\,, \qquad \mathbf{m} = \mathbf{A}\,\frac{\partial \psi(S,\boldsymbol{\Gamma},\boldsymbol{\Omega})}{\partial \boldsymbol{\Omega}}$$

$$\frac{\partial \mathbf{n}}{\partial S} + \bar{\mathbf{n}} = A_\rho\,\ddot{\boldsymbol{\phi}}_o$$

$$\frac{\partial \mathbf{m}}{\partial S} + \frac{\partial \boldsymbol{\phi}_o}{\partial S} \times \mathbf{n} + \bar{\mathbf{m}} = \mathbf{I}_\rho\,\dot{\mathbf{w}} + \mathbf{w} \times [\mathbf{I}_\rho\,\mathbf{w}]$$

The function $\psi(S, \boldsymbol{\Gamma}, \boldsymbol{\Omega})$ corresponds to the constitutive law relating the strain measures $\boldsymbol{\Gamma}$ and $\boldsymbol{\Omega}$ to the internal forces $\mathbf{n}$ and $\mathbf{m}$. We often assume in practice

$$\psi(S, \boldsymbol{\Gamma}, \boldsymbol{\Omega}) = \frac{1}{2}\begin{Bmatrix} \boldsymbol{\Gamma} \\ \boldsymbol{\Omega} \end{Bmatrix} \cdot \mathbf{C} \begin{Bmatrix} \boldsymbol{\Gamma} \\ \boldsymbol{\Omega} \end{Bmatrix}, \tag{2.4}$$

with

$$\mathbf{C} := Diag[GA_1,\, GA_2,\, EA,\, EI_1,\, EI_2,\, GJ]\,, \tag{2.5}$$

where GA_1 and GA_2 denote respectively the shear stiffness along $\mathbf{t}_1$ and $\mathbf{t}_2$, EA the axial stiffness, EI_1 and EI_2 the principal bending stiffness relative to axes $\mathbf{t}_1$ and $\mathbf{t}_2$, respectively. in Box 1, $A_\rho := \int_\Omega \rho_o\, d\Omega$, is the mass per unit length of the beam, where ρ_o denotes the mass density. Let $\mathbb{I}_\rho = \mathbb{I}_{IJ}\mathbf{E}_I \otimes \mathbf{E}_J$ be the inertia

dyadic (constant with respect to time) of the cross section in the reference configuration given by

$$\mathbf{I}_\rho(S) := \mathbf{I}_{\alpha\beta}(S)\,[\delta_{\alpha\beta}\,\mathbf{1}_3 - \mathbf{E}_\alpha \otimes \mathbf{E}_\beta]\,, \qquad \mathbf{I}_{\alpha\beta}(S) := \int_{\Omega(S)} \rho_o(S)\, X_\alpha\, X_\beta\, d\Omega\dagger \quad (2.6)$$

Further, introduce the time dependent spatial tensor $\mathbf{I}_\rho = \mathbf{I}_{\alpha\beta}\mathbf{e}_\alpha \otimes \mathbf{e}_\beta$ such that $\mathbf{I}_\rho(S,t) = \mathbf{A}(S,t)\,\mathbf{I}_\rho(S)\,\mathbf{A}^T(S,t)$.

3. Dynamics of flexible satellites

Mathematically, the system of partial differential equations summarized in Box 1 completely describes the dynamics of a flexible satellite constituted of beam elements. However, from the computational standpoint, such formulation becomes numerically ill-conditioned when the dynamics is referred directly to the inertial frame. The reason of this ill-conditioning becomes clear when comparing the magnitude of structural deformations with the distance from the satellite to the center of the earth. Owing to the property of invariance with respect to superposed rigid body motion of the proposed rod model, we can refer the dynamics of the satellite to a parallel translate of the inertial frame, which describes properly the structural deformation when its origin is placed in the neighborhood of the satellite.

3.1. Rotationally-fixed floating frame

We introduce the frame $\{Z;\mathbf{a}_1, \mathbf{a}_2, \mathbf{a}_3\}$, as shown in Figure 3.1, with base point $Z \in \mathbb{R}^3$ whose position relative to origin O of the inertial frame is given by the position vector

$$\mathbf{Z}(t) = Z_i(t)\,\mathbf{e}_i\,, \quad (3.1)$$

and such that the orthonormal basis vectors $\{\mathbf{a}_i\}$ have constant components relative to the inertial basis $\{\mathbf{e}_i\}$. This frame is thus rotationally-fixed with respect to the inertial frame, and will be henceforth referred to as the *rotationally-fixed floating frame.* For convenience, we choose $\mathbf{a}_k \equiv \mathbf{e}_k \equiv \mathbf{E}_k$, which makes $\{Z;\mathbf{e}_1, \mathbf{e}_2, \mathbf{e}_3\}$ to be simply a parallel translate of the inertial frame $\{O;\mathbf{e}_1, \mathbf{e}_2, \mathbf{e}_3\}$. Let $\boldsymbol{\phi}_o^Z:[0, L]\to\mathbb{R}^3$ denote the deformation map of the line of centroids of the beam relative to this frame. The position vector $\mathbf{x}_o$ in (2.1b) can now be restated in terms of $\boldsymbol{\phi}_o^Z$ as

$$\mathbf{x}_o \equiv \boldsymbol{\phi}_o(S,t) = \mathbf{Z}(t) + \boldsymbol{\phi}_o^Z(S,t) = [Z_i(t) + \phi_{oi}^Z(S,t)]\,\mathbf{e}_i \quad (3.2)$$

† Subscripts in greek letters take values in {1,2}, while subscripts in roman letters take values in {1,2,3}.

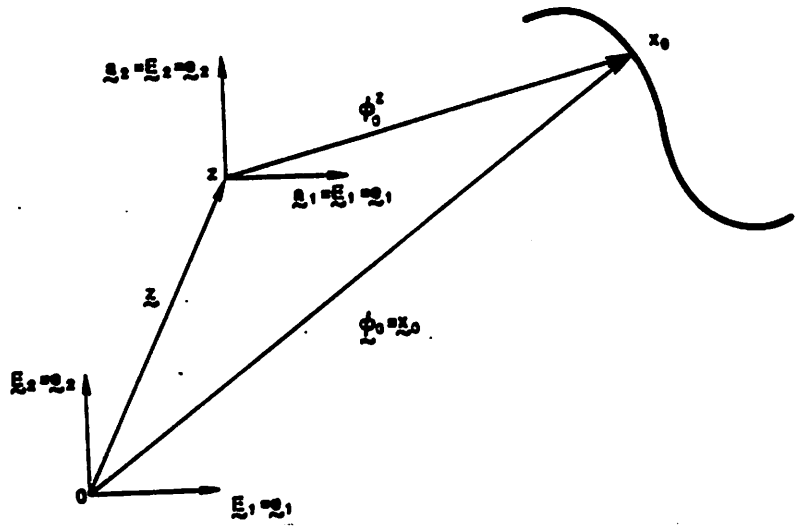

Figure 3.1. *Rotationally-fixed floating frame: parallel translate of inertial frame.*

Note that the relation (2.1c) for the rotation field remains unchanged for the rotationally-fixed floating frame. We shall refer to the map $t \rightarrow \mathbf{Z}(t)$ as the *far-field* dynamics which will be used later to describe the position of the satellite relative to the inertial frame. By the dynamics of the *near field*, we refer to the map $t \rightarrow \boldsymbol{\phi}_o^Z(S,t)$ which describes the structural deformation.

3.2. Loading conditions and far-field dynamics

Loading conditions. Three types of loading are considered. The simplest loading is the spatially fixed type with (possibly time varying) components relative to the inertial basis vectors given by $\bar{\mathbf{n}}^f(t) = n_i^f(t)\, \mathbf{e}_i$. Most relevant to flexible satellites is loading which is dependent on the deformation of the structures, such as actuator control force — coming, for example, from gaz jets or ion thrusters — used for the pointing maneuver and vibration suppression. The actuator control force considered herein falls into the category of follower loading of the circulatory type — that is, loading which is not derivable from a potential and not explicitly dependent on time — defined as follows

$$\bar{\mathbf{n}}^a(t) := N_I^a(t)\, \mathbf{t}_I(t)\,. \tag{3.3a}$$

The applied load in (3.3a) thus follows the change in orientation of the cross section, represented by the basis $\{\mathbf{t}_I\}$, and may have time varying magnitude. By virtue of (2.1c), relation (3.3a) can be rewritten as

$$\bar{\mathbf{n}}^a(\mathbf{\Lambda}) = \Lambda_{iI}\, N_I^a\, \mathbf{e}_i\,, \tag{3.3b}$$

thus expliciting the dependence of the actuator loading on the configuration. Finally, gravity loading derived from spherical potential applied to a material

point of mass A_ρ located at a distance $\boldsymbol{\phi}_o$ from the source, here the origin O, of the form

$$\bar{\mathbf{n}}^g(\boldsymbol{\phi}_o) = -\frac{A_\rho\,\mu\,\boldsymbol{\phi}_o}{\|\boldsymbol{\phi}_o\|^3} \tag{3.4}$$

is also configuration dependent. In (3.4), μ denotes the gravitational constant. For the rod model, using (3.4) implies the reasonable assumption that the mass of the rod is concentrated on the line of centroids. Although more complex models of the gravitation field could be considered, our purpose here is to show how the formulation could accommodate configuration dependent loading. For this reason, within the scope of this paper, we shall consider only the following type of loading

$$\bar{\mathbf{n}} = \bar{\mathbf{n}}^f + \bar{\mathbf{n}}^a(\mathbf{A}) + \bar{\mathbf{n}}^g(\boldsymbol{\phi}_o) \tag{3.5}$$

Far-field dynamics. To determine the far field dynamics $t \to \mathbf{Z}(t)$, we shall employ the following equation which defines the motion of the center of mass of the satellite,

$$\ddot{\mathbf{Z}}(t) = \mathbf{f}(\mathbf{Z}, \mathbf{A}) := \frac{\mu\,\mathbf{p}}{\|\mathbf{Z}\|^2} + \frac{1}{M}\int_{[0,\,L]} [\bar{\mathbf{n}}^f + \bar{\mathbf{n}}^a(\mathbf{A})]\,dS\,, \tag{3.6a}$$

where $\mathbf{p}$ is the unit vector defined as $\mathbf{p} := \dfrac{\mathbf{Z}}{\|\mathbf{Z}\|}$, and M the total mass of the satellite,

$$M := \int_{[0,\,L]} A_\rho(S)\,dS \tag{3.6b}$$

The first term on the right-hand side of (3.6a) gives the acceleration due to the gravitational field, whereas the second term represents the acceleration produced by the spatially fixed and actuator follower forces applied on the satellite.

3.3. Near-field dynamics and weak formulation

Near-field dynamics. In treating the dynamics of the near field one can always assume that the far field $t \to \mathbf{Z}(t)$ is known. The equations of motion for the near field are in fact valid for any known function $\mathbf{Z}(t)$. Noting that $\dfrac{\partial \boldsymbol{\phi}_o}{\partial S} \equiv \dfrac{\partial \boldsymbol{\phi}_o^Z}{\partial S}$ and using the decomposition (3.2), i.e., $\boldsymbol{\phi}_o(S,t) = \mathbf{Z}(t) + \boldsymbol{\phi}_o^Z(S,t)$, we obtain

$$\begin{aligned} &\frac{\partial \mathbf{n}}{\partial S} + [\,\bar{\mathbf{n}}^f + \bar{\mathbf{n}}^a(\mathbf{A}) + \bar{\mathbf{n}}^g(\mathbf{Z}, \boldsymbol{\phi}_o^Z) - A_\rho\,\ddot{\mathbf{Z}}\,] = A_\rho\,\ddot{\boldsymbol{\phi}}_o^Z \\ &\frac{\partial \mathbf{m}}{\partial S} + \frac{\partial \boldsymbol{\phi}_o^Z}{\partial S} \times \mathbf{n} + \bar{\mathbf{m}} = \mathbf{I}_\rho\,\dot{\mathbf{w}} + \mathbf{w} \times [\mathbf{I}_\rho\,\mathbf{w}] \end{aligned} \tag{3.7a}$$

The strain measure $\boldsymbol{\Gamma}$ is now evaluated by

$$\boldsymbol{\Gamma} = \mathbf{A}^T \frac{\partial \boldsymbol{\phi}_o^Z}{\partial S} - \mathbf{E}_3 \tag{3.7b}$$

It is noted that equations concerning the dynamics of the rotation field of the rod and its curvature in BOX 1 remain identically the same in above formulation.

In all applications of interest, the origin Z of the rotationally-fixed floating frame, with position vector $\mathbf{Z}(t)$, is located in a small neighborhood of the center of mass. For this situation we have $\epsilon := \dfrac{\|\boldsymbol{\phi}_o^Z\|}{\|\mathbf{Z}\|} \ll 1$. To avoid numerical ill-conditioning of the gravitational force field $\bar{\mathbf{n}}^g(\mathbf{Z}, \boldsymbol{\phi}_o^Z)$, one employs the following standard Taylor series expansion that retains terms up to order $O(\epsilon^2)$

$$\bar{\mathbf{n}}^g(\mathbf{Z}, \boldsymbol{\phi}_o^Z) \equiv -A_\rho \mu \frac{\boldsymbol{\phi}_o^Z + \mathbf{Z}}{\|\boldsymbol{\phi}_o^Z + \mathbf{Z}\|^3} = -\frac{A_\rho \mu \boldsymbol{\phi}_o^Z}{\|\mathbf{Z}\|^3}\left[1 - \frac{3\,\mathbf{p}\bullet\boldsymbol{\phi}_o^Z}{\|\mathbf{Z}\|}\right]$$
$$-\frac{A_\rho \mu \mathbf{p}}{\|\mathbf{Z}\|^2}\left[1 - \frac{3\,\mathbf{p}\bullet\boldsymbol{\phi}_o^Z}{\|\mathbf{Z}\|} - \frac{3}{2}\frac{\|\boldsymbol{\phi}_o^Z\|^2}{\|\mathbf{Z}\|^2} + \frac{15}{2}\frac{(\mathbf{Z}\bullet\boldsymbol{\phi}_o^Z)^2}{\|\mathbf{Z}\|^4}\right] + \mathrm{O}(\epsilon^3)\,. \tag{3.8}$$

Remark 3.1. It should be noted that the far-field dynamics and the near-field dynamics are coupled through the presence of follower actuator force $\bar{\mathbf{n}}^a(\mathbf{A})$, dependent on the rotation field $\mathbf{A}$ of the rod, in equation (3.6) and the presence of the forcing term $A_\rho \ddot{\mathbf{Z}}$ as well as the gravity force $\bar{\mathbf{n}}^g(\mathbf{Z}, \boldsymbol{\phi}_o^Z)$, which depends on the far field $\mathbf{Z}(t)$, in equation (3.7). □

Dynamic weak-form of the near field. The weak formulation (virtual work statement) of the local equations (3.7) governing the dynamics of the near field is the corner stone of the finite element numerical solution procedure discussed in the next section. Consider a configuration of the satellite defined by $\boldsymbol{\phi}_o(S, t) = \mathbf{Z}(t) + \boldsymbol{\phi}_o^Z(S, t)$ and $\mathbf{A}(S, t)$. We shall denote by $S \to \boldsymbol{\eta}(S) := (\boldsymbol{\eta}_o(S), \boldsymbol{\psi}(S))$ an *admissible variation* of the configuration $\boldsymbol{\phi} := (\boldsymbol{\phi}_o^Z, \mathbf{A})$. Physically, $S \to \boldsymbol{\eta}_o(S)$ represents a superposed infinitesimal displacement field, and $S \to \boldsymbol{\psi}(S)$ a superposed infinitesimal rotation field onto the satellite. By multiplying (3.7) by $\boldsymbol{\eta}(S)$ and integrating over $[0, L]$ we obtain, after integration by parts, the following dynamic weak form

$$G_{dyn}(\boldsymbol{\phi}, \boldsymbol{\eta}) := \int_{[0, L]} \{A_\rho \ddot{\boldsymbol{\phi}}_o^Z \bullet \boldsymbol{\eta}_o + [\mathbf{I}_\rho \dot{\mathbf{w}} + \mathbf{w} \times (\mathbf{I}_\rho \mathbf{w})] \bullet \boldsymbol{\psi}\}\, dS - G(\boldsymbol{\phi}, \boldsymbol{\eta}) \tag{3.9a}$$

Here, $G(\boldsymbol{\phi}, \boldsymbol{\eta})$ denotes the static weak form of equilibrium given by

$$G(\boldsymbol{\phi}, \boldsymbol{\eta}) := \int_{[0, L]} \{\mathbf{n} \bullet [\frac{\partial \boldsymbol{\eta}_o}{\partial S} - \boldsymbol{\psi} \times \frac{\partial \boldsymbol{\phi}_o^Z}{\partial S}] + \mathbf{m} \bullet \frac{\partial \boldsymbol{\psi}}{\partial S}\}\, dS - G_{ext}(\boldsymbol{\phi}, \boldsymbol{\eta}) \tag{3.9b}$$

where $G_{ext}(\boldsymbol{\phi}, \boldsymbol{\eta})$ is the weak form of the externally applied loading; that is

$$G_{ext}(\boldsymbol{\phi}, \boldsymbol{\eta}) := \int_{[0, L]} \{[\, \bar{\mathbf{n}}^f + \bar{\mathbf{n}}^g(\mathbf{Z}, \boldsymbol{\phi}_o^Z) + \bar{\mathbf{n}}^a(\mathbf{A}) - A_\rho \ddot{\mathbf{Z}}\,] \cdot \boldsymbol{\eta}_o + \bar{\mathbf{m}} \cdot \boldsymbol{\psi}\} dS \,. \quad (3.10)$$

It is noted that in (3.10), the far field $\mathbf{Z}(t)$ is assumed to be known, and the acceleration term $A_\rho \ddot{\mathbf{Z}}$ is regarded as an additional forcing term.

4. Computational solution strategy

In this section, we shall state the coupled problem to be solved and discuss in detail the numerical integration procedure. The proposed treatment relies on an essential property of our formulation: The motion of the rotationally-fixed floating frame relative to the satellite (the map $t \to \mathbf{Z}(t)$), in strict mathematical consideration, has absolutely no influence on the mechanical behavior of the satellite (the deformation map $t \to \boldsymbol{\phi}_o^Z(S,t)$). Its role in the formulation can be thought of simply as a "zooming device," and serves the sole practical purpose of avoiding numerical ill-conditioning resulting from the large difference in magnitude between the structural deformation and the distance from the satellite to the center of the earth. This ill-conditioning of course arises only when gravitational force is taken into account in the formulation.

Conceptually, the coupled problem to be solved may be stated as

Find $\mathbf{Z}(t)$, $\boldsymbol{\phi}_o^Z(S, t)$, *and* $\mathbf{A}(S, t)$ *such that:*
$\ddot{\mathbf{Z}} = \mathbf{f}(\mathbf{Z}, \mathbf{A})$, *and*
$G_{dyn}(\boldsymbol{\phi}, \boldsymbol{\eta}) = 0$, *for any* $\boldsymbol{\eta}$ *admissible,*

where $\boldsymbol{\phi} := (\boldsymbol{\phi}_0, \mathbf{A})$, and $\boldsymbol{\phi}_0 = \mathbf{Z} + \boldsymbol{\phi}_o^Z$. The single-step solution procedure can be summarized as follows:

> *Assume that at time* $t = t_n$, *the solution is known, i.e., we have solved for* $\{\mathbf{Z}(t_n), \boldsymbol{\phi}_o^Z(S,t_n), \mathbf{A}(S,t_n)\}$. *Find the solution at time* $t_{n+1} = t_n + h$ *denoted by* $\{\mathbf{Z}(t_{n+1}), \boldsymbol{\phi}_o^Z(S,t_{n+1}), \mathbf{A}(S,t_{n+1})\}$, *where* h *represents the time step size, based only on the known solution at time* t_n.

We propose a single-step explicit/implicit transient algorithm to solve the above coupled far-field/near-field satellite dynamics problem. Consider the time interval of interest $[0, T]$ to be discretized into subintervals such that $[0, T] = \bigcup_{n \geq 0} [t_n, t_{n+1}]$, where $t_{n+1} := t_n + h$, and h is the time-step size. The following steps are performed over the interval $[t_n, t_{n+1}]$:

(i) Solve the initial value problem $\ddot{\mathbf{Z}} = f(\mathbf{Z}, \mathbf{A})$, with initial condition $\mathbf{Z}(t_n) = \mathbf{Z}_n$, by *assuming that* $\mathbf{A}$ *remains unchanged within this time interval,*

i.e., $\mathbf{A}(S,t) \equiv \mathbf{A}(S, t_n)$, *for* $t \in [t_n, t_{n+1}]$. The numerical integration is performed by an *explicit* integration method.

(ii) Solve the *nonlinear structural dynamic problem* $G_{dyn}(\boldsymbol{\phi}, \boldsymbol{\eta}) = 0$ by a generalized Newmark *implicit* time-stepping algorithm and the spatial Galerkin finite element method. This discretization procedure results in a system of nonlinear algebraic equations that can be solved by Newton's method.

We shall first discuss in Section **4.1** the temporal discretization in steps (i) and (ii), followed by the spatial Galerkin finite element discretization of the weak form for the near-field in Section **4.2**.

4.1. Temporal discretization

In line with standard usage, we employ the subscript n to denote the temporal discrete approximate of a time-varying quantity at time t_n; thus for the far field $\mathbf{Z}_n \cong \mathbf{Z}(t_n)$, for the near field $\mathbf{d}_n(S) \cong \boldsymbol{\phi}_o^Z(S,t_n)$, $\mathbf{v}_n(S) \cong \dot{\boldsymbol{\phi}}_0^Z(S,t_n)$, $\mathbf{a}_n(S) \cong \ddot{\boldsymbol{\phi}}_o^Z(S,t_n)$, and for the rotation field $\mathbf{A}_n(S) \cong \mathbf{A}(S,t_n)$, $\mathbf{w}_n(S) \cong \mathbf{w}(S,t_n)$, $\boldsymbol{\alpha}_n(S) \cong \dot{\mathbf{w}}(S,t_n)$. Also denote the configuration at time t_n as $\boldsymbol{\phi}_n(S) := (\mathbf{d}_n(S), \mathbf{A}_n(S))$.

Far-field dynamics: Explicit scheme. The ordinary differential equation (ODE) describing the motion of the center of mass of the satellite given in (3.8) is easily solved by employing any of the classical explicit single-step algorithms for ODE's (e.g., Gear [1971]) if the function $\mathbf{f}(\mathbf{Z}, \mathbf{A})$ is explicitly known. However, the dynamics of the rotation field $t \to \mathbf{A}(S,t)$ for $t \geq t_n$ is not known until we have solved the equations of motion (3.7). Hence, to solve for $\mathbf{Z}_{n+1}$, with known solution $\{\mathbf{Z}_n, \mathbf{A}_n(S)\}$, we *assume that* $\mathbf{A}(S,t) \equiv \mathbf{A}_n(S)$, *for all time* t *in the interval* $[t_n, t_{n+1}]$. In the implementation, we employ the explicit Runge-Kutta 4th order method.

Remark 4.1. A wide choice of numerical algorithms for ODE's — explicit or implicit, single-step or multi-step — could be used to solve for the far field with the above assumption. In general, due to structural vibration, the time step size of the whole numerical integration scheme is rather governed by the near-field dynamics. □

Remark 4.2. Numerical integration of the far-field dynamics is only necessary when external forces from other than the (spherical) gravitational field are applied on the satellite. In the absence of these applied forces, one can use well-known analytical solutions in orbital mechanics (the two-body problem) to obtain directly the solution for the far field $\mathbf{Z}(t)$. □

Remark 4.3. Because of the assumption that follower load remains constant in the interval $[t_n, t_{n+1}]$ for the integration of the far-field, the origin Z of the rotationally-fixed floating frame will not exactly follow the path of the center

of mass of the satellite, and could gradually drift away from the latter. We note that the assumption of piecewise constant applied follower loading used in the integration of the far field is closely related to the rectangular integration rule. This assumption can be viewed as a convenient interpolation of the follower actuator load; the role of this interpolation is to allow a decoupling in the numerical treatment of the coupled far field/near field problem. However, first due to the small time step size to accommodate structural vibration, the drift of origin Z from the center of mass would be insignificant. Second, since one could always arbitrarily reposition the floating frame relative to the satellite as will be shown later, the drift of Z from the center of mass is therefore inconsequential as far as the structural response of the satellite is concerned. □

Near-field dynamics: Implicit scheme. The basic problem concerning the discrete time-stepping algorithm for the near field may be formulated as follows. With $\mathbf{Z}_{n+1}$ known from solving the far-field dynamics as described above, and given the configuration $\boldsymbol{\phi}_n := (\mathbf{d}_n, \mathbf{A}_n)$ at time t_n, its associated linear and angular velocities, $(\mathbf{v}_n, \mathbf{w}_n)$, and linear and angular accelerations $(\mathbf{a}_n, \boldsymbol{\alpha}_n)$, obtain the configuration $\boldsymbol{\phi}_{n+1} := (\mathbf{d}_{n+1}, \mathbf{A}_{n+1})$ at time t_{n+1}, the associated linear and angular velocities $(\mathbf{v}_{n+1}, \mathbf{w}_{n+1})$, and the linear and angular acceleration $(\mathbf{a}_{n+1}, \boldsymbol{\alpha}_{n+1})$, in a manner that is (a) *consistent* and (b) *stable* † with the dynamic weak form $G_{dyn}(\boldsymbol{\phi}, \boldsymbol{\eta})$.

To this end, we proposed the generalized implicit Newmark algorithm summarized in Box 2 below. Note that the algorithm for the translational part of the configuration, that is $(S, t) \to \boldsymbol{\phi}_o^Z(S; t) \in \mathbb{R}^3$, is the classical Newmark algorithm of nonlinear elastodynamics (see, e.g., Belytschko & Hughes [1983]). The proposed algorithm for the rotational part $(S, t) \to \mathbf{A}(S, t) \in SO(3)$, in its material version, furnishes the canonical extension of the Newmark formulas to the group of orthogonal matrices describing the rotation field of the rod. In Box 2, β and τ are the Newmark parameters, and correspond to the trapezoidal rule when $\beta = \frac{1}{4}$ and $\tau = \frac{1}{2}$. Detailed discussion of the above algorithm is lengthy and falls out of the scope of the present paper. We refer to Simo & Vu-Quoc [1986a] for a geometric interpretation, the error analysis as well as the incremental form of this algorithm.

Remark 4.4. The accuracy of the implicit integration scheme for the near field is independent from the accuracy of the integration scheme for the far field

† The notion of stability corresponds essentially to well-posedness of the semi-discrete problem. In the nonlinear case the appropriate concept of stability remains unsettled, and several notions of stability have been proposed (A-stability, spectral stability, stability in the energy sense, stiffly-stable methods, etc...). See, e.g., Hughes [1976], or Belytschko & Hughes [1983].

BOX 2. *Generalized implicit Newmark algorithm*

Momentum Balance at t_{n+1}	
$G_{dyn}(\boldsymbol{\phi}_{n+1}, \boldsymbol{\eta}) = 0$, for all $\boldsymbol{\eta}$ admissible	
Translation	**Rotation**
$\mathbf{d}_{n+1} := \mathbf{d}_n + \mathbf{u}_n$	$\mathbf{A}_{n+1} := \mathbf{A}_n \exp[\, \mathbf{A}_n^T \overset{\mathrm{v}}{\boldsymbol{\theta}}_n \mathbf{A}_n \,]$
$\mathbf{u}_n := h\,\mathbf{v}_n + h^2\,[(\frac{1}{2} - \beta)\,\mathbf{a}_n + \beta\,\mathbf{a}_{n+1}]$	$\overset{\mathrm{v}}{\boldsymbol{\theta}}_n := h\,\overset{\mathrm{v}}{\mathbf{w}}_n + h^2\,[(\frac{1}{2} - \beta)\,\overset{\mathrm{v}}{\boldsymbol{\alpha}}_n + \beta\,\overset{\mathrm{v}}{\boldsymbol{\alpha}}_{n+1}]$
$\mathbf{v}_{n+1} := \mathbf{v}_n + h\,[(1 - \tau)\,\mathbf{a}_n + \tau\,\mathbf{a}_{n+1}]$	$\overset{\mathrm{v}}{\mathbf{w}}_{n+1} := \overset{\mathrm{v}}{\mathbf{w}}_n + h\,[(1 - \tau)\,\overset{\mathrm{v}}{\boldsymbol{\alpha}}_n + \tau\,\overset{\mathrm{v}}{\boldsymbol{\alpha}}_{n+1}]$

in the sense that we shall always obtain the structural displacement and rotation fields of the rod up to second order accuracy (see the analysis in Simo & Vu-Quoc [1986a]) regardless of the choice of integration scheme for the far field. □

We shall now proceed to the spatial discretization procedure of $G_{dyn}(\boldsymbol{\phi}_{n+1}, \boldsymbol{\eta})$.

4.2. Linearization and spatial discretization

We recall that as a result of introducing the generalized Newmark time stepping algorithm outlined above, the weak form $G_{dyn}(\boldsymbol{\phi}_{n+1}, \boldsymbol{\eta}) = 0$ governing the dynamics of near field becomes a nonlinear functional depending on $\boldsymbol{\phi}_{n+1}(S) := (\mathbf{d}_{n+1}(S), \mathbf{A}_{n+1}(S))$. In what follows, we shall be concerned with the spatial discretization of this nonlinear functional by a Galerkin procedure. First, we provide some detail concerning the linearization of the loading term involving the gravity load.

Tangent gravity load stiffness operator. The solution of the nonlinear variational problem $G_{dyn}(\boldsymbol{\phi}_{n+1}, \boldsymbol{\eta}) = 0$ by Newton's method — step (ii) of the solution strategy outlined above — involves the solution of a sequence of linearized problems, denoted by $L[\, G(\boldsymbol{\phi}^{(i)}_{n+1}, \boldsymbol{\eta})\,] = 0$ where the superscript (i) designates the iteration number. These linear problems are obtained by consistent linearization of $G_{dyn}(\boldsymbol{\phi}, \boldsymbol{\eta}) = 0$, at the current configuration $S \to \boldsymbol{\phi}^{(i)}_{n+1}(S)$ $:= (\mathbf{d}^{(i)}_{n+1}(S), \mathbf{A}^{(i)}_{n+1}(S))$, in the direction of an incremental field $S \to \Delta\boldsymbol{\phi}^{(i)}_{n+1}(S)$ $:= (\Delta\mathbf{u}^{(i)}_{n+1}(S), \Delta\boldsymbol{\theta}^{(i)}_{n+1}(S))$ according to the directional derivative formula

$$L[\, G_{dyn}(\boldsymbol{\phi}^{(i)}_{n+1}, \boldsymbol{\eta})\,] := G_{dyn}(\boldsymbol{\phi}^{(i)}_{n+1}, \boldsymbol{\eta}) + \frac{d}{d\epsilon}\bigg|_{\epsilon=0} G_{dyn}(\boldsymbol{\phi}^{(i)}_{n+1} + \epsilon\,\Delta\boldsymbol{\phi}^{(i)}_{n+1}, \boldsymbol{\eta}) = 0 \tag{4.1}$$

A detailed account of the linearization process for the static weak form $G(\boldsymbol{\phi}^{(i)}_{n+1}, \boldsymbol{\eta})$ defined in (3.9b) that includes consideration of follower loading is

contained in Simo & Vu-Quoc [1985b]. Extension of this methodology to the dynamic problem governed by $G_{dyn}(\phi_{n+1}^{(i)}, \eta)$ in (3.9a) is given in Simo & Vu-Quoc [1986a]. Thus, within the present context, it only remains to address the linearization of the contribution to $G_{ext}(\phi_{n+1}^{(i)}, \eta)$ defined by (3.10) of the gravity force field. This contribution will be denoted by $G_{ext}^{g}(\phi_{n+1}^{(i)}, \eta)$ in what follows. By making use of the Taylor series expansion (3.8) in (3.10), use of the directional derivative formula yields the expression

$$\frac{d}{d\epsilon}\bigg|_{\epsilon=0} G_{ext}^{g}(\phi_{n+1}^{(i)}+\epsilon\Delta\phi_{n+1}^{(i)}, \eta) = -\int_{[0,\,L]} \frac{A_\rho\ \mu\ \eta_o}{\|\mathbf{Z}_{n+1}\|^3} \cdot \left[3\left(1 - \frac{5\ \mathbf{p}_{n+1}\cdot\mathbf{d}_{n+1}^{(i)}}{\|\mathbf{Z}_{n+1}\|}\right) \mathbf{p}_{n+1}\otimes\mathbf{p}_{n+1} + \frac{3}{\|\mathbf{Z}_{n+1}\|}\,\mathbf{p}_{n+1}\otimes\mathbf{d}_{n+1}^{(i)} + \left(1 - \frac{3\ \mathbf{p}_{n+1}\cdot\mathbf{d}_{n+1}^{(i)}}{\|\mathbf{Z}_{n+1}\|}\right)\mathbf{1}_3 \right] \Delta\mathbf{u}_{n+1}^{(i)}\, dS \qquad (4.2)$$

Note that the above tangent gravity load stiffness operator is non-symmetric and involves only the translational degrees of freedom. This result will be used in the computation of the load stiffness matrix upon introducing the spatial discretization.

Spatial discretization: Galerkin finite element method. We begin by introducing a partition of the interval $[0, L]$ into non-overlapping subintervals according to $[0, L] = \bigcup_{k=1}^{N-1} [S_k, S_{k+1}]$, where $0 \equiv S_1 < S_2 < \cdots < S_N \equiv L$. Consider the following approximation for the translational field

$$\mathbf{d}_{n+1}(S) \cong \sum_{I=1}^{N} N_I(S)\,\mathbf{d}_{n+1,I}\,, \quad \text{where} \quad \mathbf{d}_{n+1,I} := \mathbf{d}_{n+1}(S_I)\,. \qquad (4.3a)$$

Here, $N_I(S)$ is a set of global functions which are either prescribed or constructed from local finite element approximations in the standard manner. An interpolation for the rotation field $S \to \mathbf{A}_{n+1}(S)$ is constructed by noting that $\mathbf{A}_{n+1}(S) = \exp[\overset{\mathrm{v}}{\boldsymbol{\chi}}_{n+1}(S)]$, where $\overset{\mathrm{v}}{\boldsymbol{\chi}}(S)$ is the skew-symmetric matrix associated with the rotation vector $\boldsymbol{\chi}$. We then consider the approximation for the rotation field

$$\boldsymbol{\chi}_{n+1}(S) \cong \sum_{I=1}^{N} N_I(S)\,\boldsymbol{\chi}_{n+1,I}\,, \quad \text{where} \quad \boldsymbol{\chi}_{n+1,I} := \boldsymbol{\chi}_{n+1}(S_I)\,,$$
$$\text{and} \quad \mathbf{A}_{n+1}(S) \cong \exp[\boldsymbol{\chi}_{n+1}(S)]\,. \qquad (4.3b)$$

Note that the approximation scheme for the rotation field preserves exactly the orthogonality property of $\mathbf{A}$. By substitution of the interpolation in (4.3a-b) into the the weak form $G_{dyn}(\phi_{n+1}, \eta) = 0$, and assuming that the incremental displacement field $\Delta\phi_{n+1}^{(i)} := (\Delta\mathbf{u}_{n+1}^{(i)}, \Delta\boldsymbol{\theta}_{n+1}^{(i)})$ and the admissible variations $\eta := (\eta_o, \psi)$ are approximated in the same manner according to

$$\Delta\boldsymbol{\phi}^{(i)}_{n+1}(S) \cong \sum_{I=1}^{N} N_I(S)\,\Delta\boldsymbol{\phi}^{(i)}_{I,n+1} \quad \text{with } \Delta\boldsymbol{\phi}^{(i)}_{I,n+1} \cong \Delta\boldsymbol{\phi}^{(i)}_{n+1}(S_I)\,, \tag{4.3c}$$

$$\boldsymbol{\eta}(S) \cong \sum_{I=1}^{N} N_I(S)\,\boldsymbol{\eta}_I \quad \text{with } \boldsymbol{\eta}_I \cong \boldsymbol{\eta}(S_I)\,, \tag{4.3d}$$

after application of standard results in variational calculus, we arrive at a system of nonlinear algebraic equations, for the unknown $\boldsymbol{\phi}^{(i)}_{n+1}$, whose linearized form is given by

$$\mathbf{P}_I(\boldsymbol{\phi}^{(i)}_{n+1}) + \sum_{J=1}^{N} \mathbf{K}_{IJ}(\mathbf{A}_n, \boldsymbol{\phi}^{(i)}_{n+1})\,\Delta\boldsymbol{\phi}^{(i)}_{n+1,J} = \mathbf{O}\,, \tag{4.4a}$$

for I=1,...,*N*. In (4.4a), $\mathbf{P}_I$ represents the residual force, and $\mathbf{K}_{IJ}$ the dynamic tangent stiffness matrix obtained from

$$\begin{aligned}\mathbf{K}_{IJ}(\mathbf{A}_n, \boldsymbol{\phi}^{(i)}_{n+1}) = \mathbf{M}_{IJ}(\mathbf{A}_n, \mathbf{A}^{(i)}_{n+1}) + \mathbf{S}_{IJ}(\boldsymbol{\phi}^{(i)}_{n+1}) + \mathbf{G}_{IJ}(\boldsymbol{\phi}^{(i)}_{n+1}) \\ + \mathbf{L}^{s}_{IJ}(\mathbf{A}^{(i)}_{n+1}) + \mathbf{L}^{g}_{IJ}(\mathbf{Z}_{n+1}, \mathbf{d}^{(i)}_{n+1})\,.\end{aligned} \tag{4.4b}$$

Expressions for the tangent inertia matrix $\mathbf{M}_{IJ}$, the material tangent stiffness matrix $\mathbf{S}_{IJ}$, the tangent geometric stiffness matrix $\mathbf{G}_{IJ}$, and the tangent follower load stiffness $\mathbf{L}^{s}_{IJ}$ have been obtained in Simo & Vu-Quoc [1986a-b], and are summarized in the Appendix. The expression for the tangent gravity load stiffness results from the introduction of the approximations (4.3a,c) into (4.2),

$$\begin{aligned}\mathbf{L}^{g}_{IJ}(\mathbf{Z}_{n+1}, \mathbf{d}^{(i)}_{n+1}) = -\int_{[0,\,L]} \frac{A_\rho\,\mu}{\|\mathbf{Z}_{n+1}\|^3} \Bigg[3\left(1 - \frac{5\,\mathbf{p}_{n+1}\bullet\mathbf{d}^{(i)}_{n+1}(S)}{\|\mathbf{Z}_{n+1}\|}\right)\mathbf{p}_{n+1}\otimes\mathbf{p}_{n+1} \\ + \frac{3}{\|\mathbf{Z}_{n+1}\|}\,\mathbf{p}_{n+1}\otimes\mathbf{d}^{(i)}_{n+1}(S) + \left(1 - \frac{3\,\mathbf{p}_{n+1}\bullet\mathbf{d}^{(i)}_{n+1}(S)}{\|\mathbf{Z}_{n+1}\|}\right)\mathbf{1}_3\Bigg]\,N_I(S)\,N_J(S)\,dS\end{aligned} \tag{4.4c}$$

The incremental displacement and rotation $\Delta\boldsymbol{\phi}^{(i)}_{n+1}$ can be obtained easily by solving (4.4a). The update procedure to obtain the solution $\boldsymbol{\phi}^{(i+1)}_{n+1}$ at iteration $(i+1)$ such that the solution always remains in the configuration manifold is, however, non-trivial; we refer to Simo & Vu-Quoc [1986a,b] for the detailed discussion.

4.3. Repositioning of the rotationally-fixed floating frame

One of the salient features of our formulation is that the rotationally-fixed floating frame could be arbitrarily repositioned and its velocity in the inertial frame reset at any time. Thus in case of a drift of the origin Z of the floating frame from the center of mass, one could easily reposition the floating frame to the center of mass by first computing the current position of the center of mass relative to Z, denoted by $\mathbf{r}$,

$$\mathbf{r}(t) = \frac{1}{M}\int_{[0,\,L]} A_\rho(S)\,\boldsymbol{\phi}^{Z}_{o}(S,t)\,dS \tag{4.5a}$$

with velocity and acceleration relative to the floating frame given by,

$$\dot{\mathbf{r}}(t) = \frac{1}{M} \int_{[0,\,L]} A_\rho(S)\, \dot{\boldsymbol{\phi}}_o^Z(S,t)\, dS\,, \tag{4.5b}$$

$$\ddot{\mathbf{r}}(t) = \frac{1}{M} \int_{[0,\,L]} A_\rho(S)\, \ddot{\boldsymbol{\phi}}_o^Z(S,t)\, dS\,. \tag{4.5b}$$

Only when $\|\mathbf{Z}\|$ and $\|\mathbf{r}\|$ are of comparable magnitude, so that loss of precision on the structural deformation may occur due to round-off error, repositioning procedure need be performed. In this case, if we wish to reposition the floating frame at time $t = \bar{t}$, we simply restart the integration of the far-field dynamics with initial conditions reset as follows:

$$\begin{aligned} \mathbf{Z}(\bar{t}) &\leftarrow [\, \mathbf{Z}(\bar{t}) + \mathbf{r}(\bar{t}) \,] \\ \dot{\mathbf{Z}}(\bar{t}) &\leftarrow [\, \dot{\mathbf{Z}}(\bar{t}) + \dot{\mathbf{r}}(\bar{t}) \,] \end{aligned} \tag{4.6a}$$

Also the near-field dynamics is reset according to

$$\begin{aligned} \boldsymbol{\phi}_o^Z(\bar{t}) &\leftarrow [\, \boldsymbol{\phi}_o^Z(\bar{t}) - \mathbf{r}(\bar{t}) \,] \\ \dot{\boldsymbol{\phi}}_o^Z(\bar{t}) &\leftarrow [\, \dot{\boldsymbol{\phi}}_o^Z(\bar{t}) - \dot{\mathbf{r}}(\bar{t}) \,] \\ \ddot{\boldsymbol{\phi}}_o^Z(\bar{t}) &\leftarrow [\, \ddot{\boldsymbol{\phi}}_o^Z(\bar{t}) - \ddot{\mathbf{r}}(\bar{t}) \,] \end{aligned} \tag{4.6b}$$

It is clear that the above repositioning procedure leaves strictly unchanged the value at time $\bar{t}$ of $\boldsymbol{\phi}_o(\bar{t}) = \mathbf{Z}(\bar{t}) + \boldsymbol{\phi}_o^Z(\bar{t})$, and hence the values of the velocity $\dot{\boldsymbol{\phi}}_o(\bar{t})$, and acceleration $\ddot{\boldsymbol{\phi}}_o(\bar{t})$. Further, this repositioning procedure is most conveniently employed when a single-step integration algorithm for ODE's is used to solve for the far field.

5. Numerical examples

We shall now give some numerical examples that involve the dynamics of flexible multibody system, the concept of rotationally-fixed frame, and the dynamics of earth-orbiting satellite to demonstrate the effectiveness and generality of the proposed formulation. All figures of the deformed shapes reported herein are given at the same scale as the geometry of the structure: There is *no artificial magnification of the structural deformation* for visualization purpose.

Example 5.1. *Flying closed-loop chain.* To demonstrate the capability of the present approach to model the dynamics of flexible multibody systems, we consider a closed-loop chain constituted of 4 flexible links interconnected by hinges as shown in Figure **5.1***a*. It is emphasized that this problem can be treated as a direct application of the proposed approach to the dynamics of flexible beams interconnected by hinges without alteration in the formulation. This is possible since the hinge conditions can be easily accounted for in the finite element formulation by simply identifying the displacement degrees of freedom of

the hinged ends, leaving free the rotational degrees of freedom. One of the links is 500 times stiffer than the other three: Link AB in Figure 5.1*a* has a bending stiffness of $EI = 10^5$, while the remaining links have a bending stiffness of $EI = 200$. The other material properties are chosen to be identical for the four links, and are listed in Figure 5.1*a*. Initially, the closed-loop chain forms a square of length 10 for each side. The whole system has no prescribed displacement boundary condition. To create a forward motion, a force is applied at end A of the stiff link AB; the overall tumbling motion of the chain is induced by a torque applied at the same end as shown together with the time history of their magnitude in Figure 5.1*a*. Figure 5.1*b* depicts the entire sequence of motion with three close-ups given in Figures 5.1*c*–*e*. A time step size of $h = 0.1$ is used throughout the analysis.

Example 5.2. *Flying flexible beam in 3-D motion.* We consider a free-free flexible beam initially placed at an inclined position and subject to applied force and torques at the lower free end as shown in Figure 5.2*a*. This example has been previously analyzed in Simo & Vu-Quoc [1986b] using the time-stepping algorithm partly summarized in Box 2, together with the Galerkin finite element method to solve the system of PDE's given in Box 1. Our purpose here is to show how the concept of decomposition of the deformation map into the far field and the near field could be employed in a simple manner. The overall translational motion of the beam results from the applied force along the axis $\mathbf{e}_1$, whereas the forward tumbling motion results from the torque about axis $\mathbf{e}_3$, and the out-of-plane motion from the applied torque about axis $\mathbf{e}_2$. These applied force and torque, of the spatially fixed type mentioned earlier, induce the free-free beam into a "kayak-rowing" motion with the early tumbling stage depicted in Figure 5.2*b*. In this Figure, finite deformation is clearly discernible. The entire sequence of motion as projected onto the plane $(\mathbf{e}_1, \mathbf{e}_2)$ is given in Figure 5.2*c*; the projection onto the plane $(\mathbf{e}_2, \mathbf{e}_3)$ in Figure 5.2*d*. Figure 5.2*e* shows the complete sequence of motion in perspective together with the trace of the upper end.

Since gravitational field is not considered in this example, and since only spatially fixed load is applied on the beam, the dynamics of the far field and the dynamics of the near field are completely decoupled:

$$\ddot{\mathbf{Z}} = \frac{1}{M} \int_{[0,\, L]} \bar{\mathbf{n}}^f(S)\, dS\,, \tag{5.1}$$

$$\frac{\partial \mathbf{n}}{\partial S} + [\, \bar{\mathbf{n}}^f - A_\rho \ddot{\mathbf{Z}}\,] = A_\rho \ddot{\boldsymbol{\phi}}_o^Z\,. \tag{5.2}$$

Substitution of (5.1) into (5.2) yields the equation of motion for the near field

$$\frac{\partial \mathbf{n}}{\partial S} + [\, \bar{\mathbf{n}}^f - \frac{A_\rho}{M} \int_{[0,\, L]} \bar{\mathbf{n}}^f(S)\, dS\,] = A_\rho \ddot{\boldsymbol{\phi}}_o^Z\,. \tag{5.3}$$

Thus, in this example, one does not need to solve for the far field if only the near-field dynamics is of prime interest. The result is shown in Figure 5.2*f* with a clear physical meaning: The motion given in Figure 5.2*e* as perceived by an inertial observer is now seen by an observer, attached to the rotationally-fixed floating frame and moving with the center of mass. A time step size of $h = 0.1$ is used in both analyses (with and without rotationally-fixed floating frame). A justification of the time step size chosen can be found in Simo & Vu-Quoc [1985a].

Example 5.3. *Satellite dynamics: Libration and orbit transfer.* Example 5.1 demonstrates how systems with flexible components connected through hinges can be analyzed with no extra effort in accounting for the constraints that arise in traditional approaches to multibody dynamics. While the analysis of the closed-loop chain in Example 5.1 is performed for the plane motion, our formulation can accommodate fully three-dimensional motion of the beam subjected to a possible state of finite deformation as shown in Example 5.2. The latter example also serves to illustrate the effectiveness of the concept of rotationally-fixed floating frame. Both of these examples, on the other hand, do not take into account the effect of gravitational load.

To illustrate the proposed methodology for solving the coupled far-field/near-field problem in the presence of gravitational force, we consider in this last example a beam of length $100\sqrt{2}$ completely contained in the plane $\{\mathbf{e}_1, \mathbf{e}_2\}$ and placed at 45^o with respect to axis $\mathbf{e}_1$. The center of mass of the beam is initially located at a distance of 7×10^6 from the center of the earth, i.e., $\mathbf{Z}(0) = 7\times10^6\,\mathbf{e}_1$. For the center of mass to describe a circular orbit, an initial velocity of $\dot{\mathbf{Z}} = 7544.1557\,\mathbf{e}_2$ is chosen; the gravitational constant being $\mu = 3.984\times10^{14}$. We are interested in capturing the librational motion resulting from the effect of gravity gradient of the orbiting satellite when the geometric configuration of the latter departs from spherical symmetry. Hence, for simplicity we choose the initial conditions for the near field to be $\boldsymbol{\phi}_o^Z(S,0) = \dot{\boldsymbol{\phi}}_o^Z(S,0) = \ddot{\boldsymbol{\phi}}_o^Z(S,0) \equiv 0$. For the rotation field of the beam, $\mathbf{A}(S,0) = \mathbf{1}_3$, $\mathbf{w}(S,0) = \boldsymbol{\alpha}(S,0) \equiv 0$. Let λ be the (libration) angle between the beam and the unit vector $\mathbf{p} := \dfrac{\mathbf{Z}}{\|\mathbf{Z}\|}$ known as the local vertical, see Figure 5.3*a*. The dynamics of libration of a uniform bar on circular orbit ($\|\mathbf{Z}\| = \textit{constant}$) is governed by the differential equation

$$\ddot{\lambda} = \frac{3\,\mu\,\sin 2\lambda}{2\,\|\mathbf{Z}\|^3} \tag{5.4}$$

The initial conditions for (5.4) that correspond to the above chosen initial conditions for the far field and the near field are given by $\lambda(0) = \dfrac{\pi}{4}$ and

$\dot{\lambda}(0) = -\frac{\|\dot{Z}(0)\|}{\|Z(0)\|}$. Figure **5.3***b* shows the evolution of the libration angle λ as obtained from the proposed approach to finite deformation satellite dynamics and from using the 4th order Runge-Kutta method to integrate (5.4); both curves are obtained with a time step size of $h = 100$ which in fact covers a complete circular orbit in about 60 steps — the orbital period for the above initial conditions of the far field is 5830 sec. With a smaller time step size, for example $h = 10$, we can exactly achieve the result as obtained from solving (5.4). In addition to the second order accuracy of the algorithm summarized in Box 2 as compared to the fourth order accuracy in the integration of (5.4), we note that the need for a smaller step size stems from the fact that the semi-discrete equations (ODE's) of the PDE's in Box 1 are actually much stiffer than (5.4).

Next, to demonstrate how a combination of loading given by (3.5) could be applied on the satellite, we consider an orbit transfer from the current circular orbit to a higher circular orbit by passing through an intermediate elliptic orbit. This orbit transfer is achieved by activating the satellite thrusters under the form of impulsive loading in two stages. First, when the satellite completes the first revolution in the low circular orbit, impulse loading with resultant in the direction of axis $\mathbf{e}_2$ is applied to induce an increase in magnitude of the velocity $\dot{\mathbf{Z}}$, and thus put the satellite into a transitory elliptic orbit as depicted in Figure **5.3***c*. The time history of the libration angle (in degree) is given in Figure **5.3***d*. Next, when the satellite reaches the apogee of this transitory orbit, impulsive thruster force, with resultant in the negative direction of axis $\mathbf{e}_2$, is again applied to put the satellite on a higher circular orbit with radius being the distance from O, the center of the earth, to the apogee of the elliptic orbit. Since the satellite tumbles on the transitory orbit, as can be seen from Figure **5.3***d*, an impulsive couple is also applied at the same time to stop the tumbling and therefore subsequently induces the satellite into a librational motion in the higher circular orbit. The radius of the higher orbit is about 1.643×10^7 with an amplitude of libration about 70° over a half librational period of about 9610sec. This result can be easily verified using (5.4).

6. Closure

We have presented a new approach to the dynamic analysis of earth-orbiting flexible satellites. The formulation relies essentially on the property of invariance with respect to superposed rigid body motions of finite-strain structural theories, leading to considerable simplification in the inertia operator of the equations of motion whereby the dynamics is referred to the inertial frame. When gravitational load is considered, this property further allows an additive decomposition of the deformation map into the far field and the near field, from which the concept of rotationally-fixed floating frame is introduced. An efficient integration

procedure was then proposed to integrate the coupled far-field/near-field dynamics. In addition, one can account for the action of follower actuator control forces, a type of configuration dependent loading of particular interest in satellite dynamics. Further, the dynamics of multibody systems composed of flexible structures interconnected through hinges constitutes a class of problems solvable by the proposed methodology. Finally, we recall that large deformations in the structures are automatically accounted for in the formulation, and there is absolutely no restriction on the speed of evolution of the systems: all physically relevant phenomena are properly represented.

Acknowledgements. This work was performed under the auspices of the Air Force Office of Scientific Research. L. Vu-Quoc was supported by grant No. AFOSR-83-0361. This support as well as the encouragement from Professors K.S. Pister, E. Polak, and R.L. Taylor are gratefully acknowledged.

References

Argyris, J.H., "An excursion into large rotations," *Comp. Meth. Appl. Mech. Engng*, **32**, 85-155.

Belytschko, T., and T.J.R. Hughes [1983], *Computational Methods for Transient Analysis*, Elsevier Science Publishers.

Benson, D.J., and J.O. Hallquist [1985], "A simple rigid body algorithm for structural dynamics program. Part I," *Proc. of the Int. Conf. on Numerical Methods in Engineering Theory and Applications*, Swansea, Ed. by J. Middleton & G.N. Pande, A.A. Balkema Publishers, Netherlands.

Canavin, J.R., and P.W. Likins [1977], "Floating reference frames for flexible spacecrafts," *J. of Spacecrafts*, **14**(12), 724-732.

Dubowsky, S. [1985], "Active control of mechanical systems: The state-of-the-art for robotic manipulator," *Proc. of the 26th Structures, Structural Dynamics, and Material Conference*, Part 2, Orlando, Florida.

Gear, C.W. [1971], *Numerical Initial Value Problems in Ordinary Differential Equations*, Prentice-Hall, Englewood Cliffs, New Jersey.

Goldstein, H. [1980], *Classical Mechanics*, second edition, Addison Wesley, Reading, Massachusetts.

Hooker, W.W., and G. Margulies [1965], "The dynamical attitude equations for an n-body satellite," *The J. of the Astronautical Sciences*, **12**, 123-128.

Hughes, T.J.R. [1976], "Stability, convergence and growth and decay of energy of the average acceleration method in nonlinear structural dynamics," *Computers & Structures*, **6**, 313-324.

Huston, R.L. [1981], "Multibody dynamics including the effects of flexibility and compliance," *Computers & Structures*, **14**(5-6), 443-451.

Kane T.R., and D.A. Levinson [1983], "Multibody dynamics," *J. of Applied Mechanics*, **50**, 1071-1078.

Kline, R.L. [1979], "Construction of large space structures," *The J. of the Astronautical Sciences*, **27**(4), 401-418.

Roberson, R.E., and J. Wittenburg [1967], "A dynamical formalism for an arbitrary number of interconnected rigid bodies with reference to the problem of satellite attitude control," *Proc. of the 3rd Int. Congress on Automatic Control*, Butterworth and Co., Ltd, London.

Simo, J.C. [1985], "A finite strain beam formulation. The three-dimensional dynamic problem. Part I," *Comp. Meth. Appl. Mech. Engng*, **49**, 55-70.

Simo, J.C., and L. Vu-Quoc [1985], *On The Dynamics of Flexible Beams Under Large Overall Motions — The Plane Case*, Electronics Research Laboratory Memorandum No. UCB/ERL M85/63, University of California, Berkeley, August. (Submitted for publication.)

Simo, J.C., and L. Vu-Quoc [1986a], *On The Dynamics of Finite-Strain Rods Undergoing Large Motions — The Three Dimensional Case*, Electronics Research Laboratory Memorandum No. UCB/ERL M86/11, University of California, Berkeley, January. (Submitted for publication.)

Simo, J.C., and L. Vu-Quoc [1986b], "Three-dimensional finite-strain rod model. Part II: Computational aspects," *Comp. Meth. Appl. Mech. Engng*, 1986. (In press.)

Simo, J.C., and L. Vu-Quoc [1986c], *The Role of Nonlinear Theories in the Dynamics Analysis of Rotating Structures*, Electronics Research Laboratory Memorandum UCB/ERL M86/10, University of California, Berkeley, January. (Submitted for publication.)

Appendix: Finite element matrices

We summarize in this Appendix the expressions for the tangent matrices appeared in equations (4.4a-b).

Residual force.

$$\mathbf{P}_{\mathrm{I}}(\phi^{(i)}_{n+1}) = \int_{[0,\,L]} [N_{\mathrm{I}}(S)\mathbf{1}_6] \begin{Bmatrix} A_\rho\, \mathbf{a}^{(i)}_{n+1} \\ \mathbf{I}^{(i)}_{\rho,n+1}\boldsymbol{\alpha}^{(i)}_{n+1} + \mathbf{w}^{(i)}_{n+1} \times [\mathbf{I}^{(i)}_{\rho,n+1}] \end{Bmatrix} dS$$

$$+ \int_{[0,\,L]} \left[\{\Xi(\phi^{(i)}_{n+1})[N_{\mathrm{I}}(S)\mathbf{1}_6]\}^T \begin{Bmatrix} \mathbf{n}^{(i)}_{n+1} \\ \mathbf{m}^{(i)}_{n+1} \end{Bmatrix} - [N_{\mathrm{I}}(S)\mathbf{1}_6] \begin{Bmatrix} \overline{\mathbf{n}}(t_{n+1}) \\ \overline{\mathbf{m}}(t_{n+1}) \end{Bmatrix} \right] dS\,, \quad \text{(A.1a)}$$

where the differential operator Ξ is defined as

$$\Xi(\phi) := \begin{bmatrix} \frac{d}{dS}\mathbf{1}_3 & [\phi_o'\ \times] \\ \mathbf{O} & \frac{d}{dS}\mathbf{1}_3 \end{bmatrix}, \quad \text{and } \frac{d}{dS}\mathbf{1}_3 := Diag[\frac{d}{dS}, \frac{d}{dS}, \frac{d}{dS}] \tag{A.1b}$$

Tangent inertia matrix. The tangent inertia matrix has the following structure

$$\mathbf{M}_{IJ}(\mathbf{A}_n, \mathbf{A}_{n+1}^{(i)}) = \begin{bmatrix} \mathbf{m}_{IJ}^{(1,1)} & \mathbf{O} \\ \mathbf{O} & \mathbf{m}_{IJ}^{(2,2)}(\mathbf{A}_n, \mathbf{A}_{n+1}^{(i)}) \end{bmatrix} \in \mathbf{R}^{6\times 6}, \tag{A.2a}$$

with

$$\mathbf{m}_{IJ}^{(1,1)} := \frac{1}{h^2\beta}\{\int_{[0,\,L]} A_\rho N_I(S) N_J(S)\, dS\}\, \mathbf{1}_3, \tag{A.2b}$$

$$\mathbf{m}_{IJ}^{(2,2)}(\mathbf{A}_n, \mathbf{A}_{n+1}^{(i)}) := \int_{[0,\,L]} \Big[-[\mathbf{A}_{n+1}^{(i)}\{\mathbf{\Pi}_\rho \mathbf{A}_{n+1}^{(i)} + \mathbf{W}_{n+1}^{(i)} \times \mathbf{\Pi}_\rho \mathbf{W}_{n+1}^{(i)}\}\times] + \frac{1}{h^2\beta}\mathbf{A}_{n+1}^{(i)}\{\mathbf{\Pi}_\rho - h\tau[\mathbf{\Pi}_\rho \mathbf{W}_{n+1}^{(i)}\times] + h\tau[\mathbf{W}_{n+1}^{(i)}\times]\mathbf{\Pi}_\rho\}\Big] \mathbf{A}_n^T \mathbf{T}(\theta_{n+1}^{(i)}) N_I(S) N_J(S) dS \tag{A.2c}$$

with $\mathbf{A} = \mathbf{A}^T\,\alpha$, $\mathbf{W} = \mathbf{A}^T\,\mathbf{w}$, and the operator $\mathbf{T}$ defined as follows

$$\mathbf{T}(\theta) := \frac{\theta \otimes \theta}{\|\theta\|^2} + \frac{\|\theta\|/2}{\tan(\|\theta\|/2)}\,[\,\mathbf{1}_3 - \frac{\theta \otimes \theta}{\|\theta\|^2}\,] - \frac{\tilde{\theta}}{2}. \tag{A.2d}$$

Tangent material stiffness matrix.

$$\mathbf{S}_{IJ}(\phi_{n+1}^{(i)}) = \int_{[0,\,L]} \{\Xi(\phi_{n+1}^{(i)})\,[N_I(S)\mathbf{1}_6]\}^T \{\mathbf{c}(\mathbf{A}_{n+1}^{(i)})\,\Xi(\phi_{n+1}^{(i)})\,[N_J(S)\mathbf{1}_6]\}\, dS, \tag{A.3}$$

where $\mathbf{c}(\phi_{n+1}^{(i)}) := \mathbf{\Pi}(\mathbf{A}_{n+1}^{(i)})\,\mathbf{C}\,\mathbf{\Pi}^T(\mathbf{A}_{n+1}^{(i)})$, and $\mathbf{\Pi}(\mathbf{A}) := Diag[\mathbf{A}, \mathbf{A}] \in \mathbf{R}^{6\times 6}$ is a block diagonal matrix.

Tangent geometric stiffness matrix.

$$\mathbf{G}_{IJ}(\phi_{n+1}^{(i)}) = \int_{[0,\,L]} \{\mathbf{T}\,[N_I(S)\mathbf{1}_6]\}^T \{\mathbf{B}(\phi_{n+1}^{(i)})\,\mathbf{T}\,[N_J(S)\mathbf{1}_6]\}\, dS, \tag{A.4a}$$

where the operator $\mathbf{T}$ and the matrix $\mathbf{B}$ are defined as

$$\mathbf{T}^T := \begin{bmatrix} \frac{d}{dS}\mathbf{1}_3 & \mathbf{O} & \mathbf{O} \\ \mathbf{O} & \frac{d}{dS}\mathbf{1}_3 & \mathbf{1}_3 \end{bmatrix}, \tag{A.4b}$$

$$\mathbf{B}(\phi) := \begin{bmatrix} \mathbf{O} & \mathbf{O} & [-\mathbf{n}\times] \\ \mathbf{O} & \mathbf{O} & [-\mathbf{m}\times] \\ [\mathbf{n}\times] & \mathbf{O} & [\mathbf{n}\otimes\phi_o' - (\mathbf{n}\cdot\phi_o')\mathbf{1}_3] \end{bmatrix}. \tag{A.4c}$$

Tangent follower load stiffness.

$$\mathbf{L}_{IJ}^s(\mathbf{A}_{n+1}^{(i)}) = \int_{[0,\,L]} \begin{bmatrix} \mathbf{O} & N_I(S)\,N_J(S)\,[\,\bar{\mathbf{n}}^a(\mathbf{A}_{n+1}^{(i)})\times] \\ \mathbf{O} & \mathbf{O} \end{bmatrix} dS\,. \square \tag{A.5}$$

Figure Captions

Figure 5.1a. *Flying closed-loop chain.* Problem data.

Figure 5.1b. *Flying closed-loop chain.* Entire sequence of motion.

Figure 5.1c. *Flying closed-loop chain.* Deformed shape at time $t = 4.8$.

Figure 5.1d. *Flying closed-loop chain.* Deformed shape at time $t = 9.6$.

Figure 5.1e. *Flying closed-loop chain.* Deformed shape at time $t = 14.4$.

Figure 5.2a. *Flying flexible beam in 3-D motion.* Problem data.

Figure 5.2b. *Flying flexible beam in 3-D motion.* Early tumbling stage.

Figure 5.2c. *Flying flexible beam in 3-D motion.* Entire sequence of motion projected on plane (e_1, e_2).

Figure 5.2d. *Flying flexible beam in 3-D motion.* Entire sequence of motion projected on plane (e_2, e_3).

Figure 5.2e. *Flying flexible beam in 3-D motion.* Perspective view of entire sequence of motion from an observer fixed in the inertial frame.

Figure 5.2f. *Flying flexible beam in 3-D motion.* Perspective view of entire sequence of motion, from an observer fixed in the parallel translate of inertial frame.

Figure 5.3a. *Satellite dynamics: Libration and orbit transfer.*

Figure 5.3b. *Satellite dynamics: Libration and orbit transfer.* Evolution of the libration angle λ on lower circular orbit.

Figure 5.3c. *Satellite dynamics: Libration and orbit transfer.* Transition from lower to higher circular orbits.

Figure 5.3d. *Satellite dynamics: Libration and orbit transfer.* Complete time history of the libration angle.

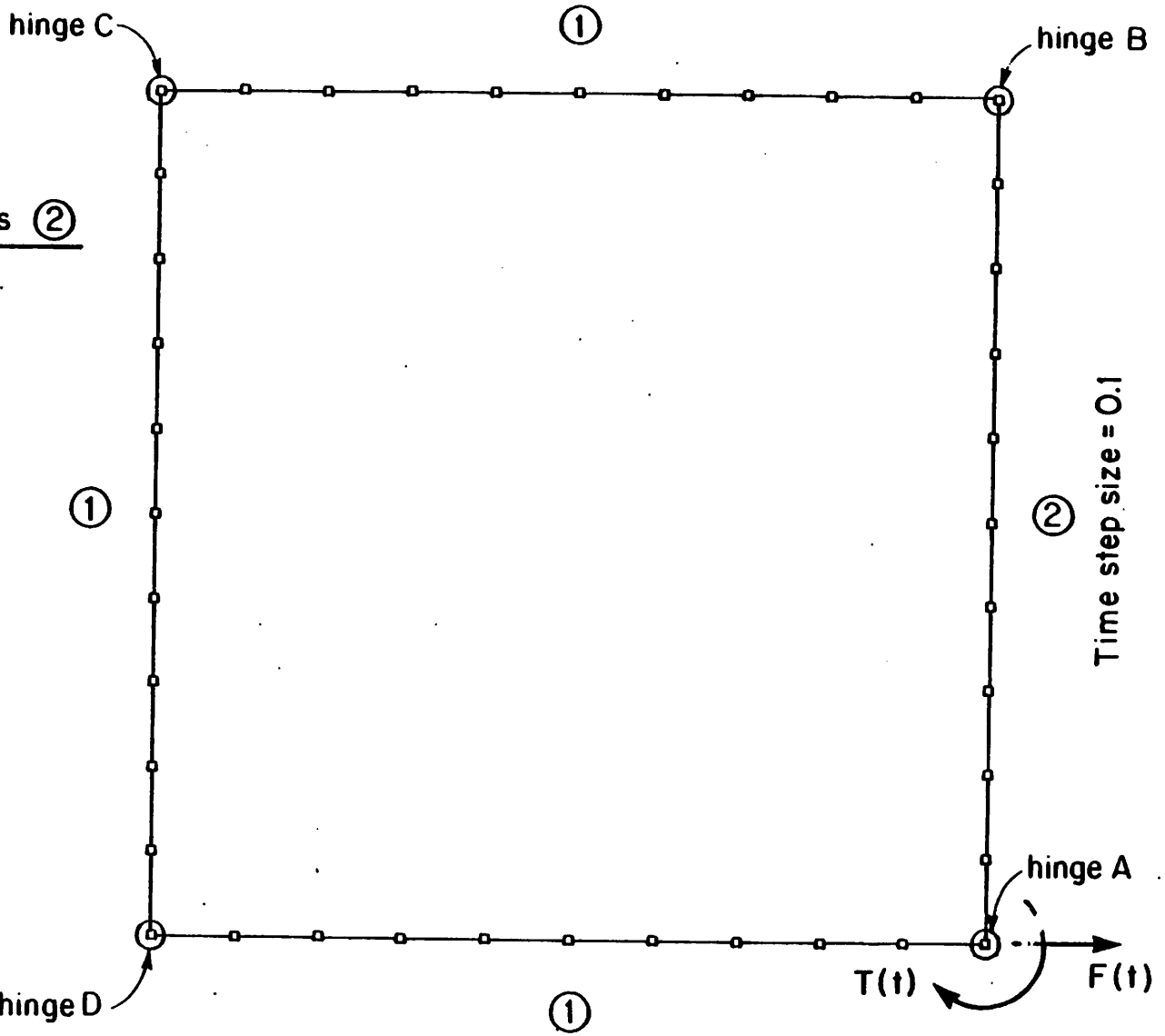

Material Properties ①

$GA_s = 10^6$
$EA = 10^6$
$EI = 200$
$A\rho = 1$
$I\rho = 10$

Material Properties ②

$GA_s = 10^6$
$EA = 10^6$
$EI = 10^5$
$A\rho = 1$
$I\rho = 10$

F.e. mesh: 40 linear elements

Time History of F(t), T(t)

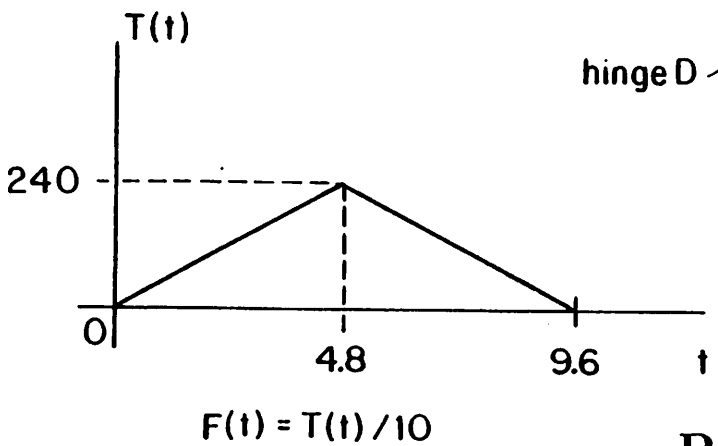

Figure 5.1a. *Flying closed-loop chain.* Problem data.

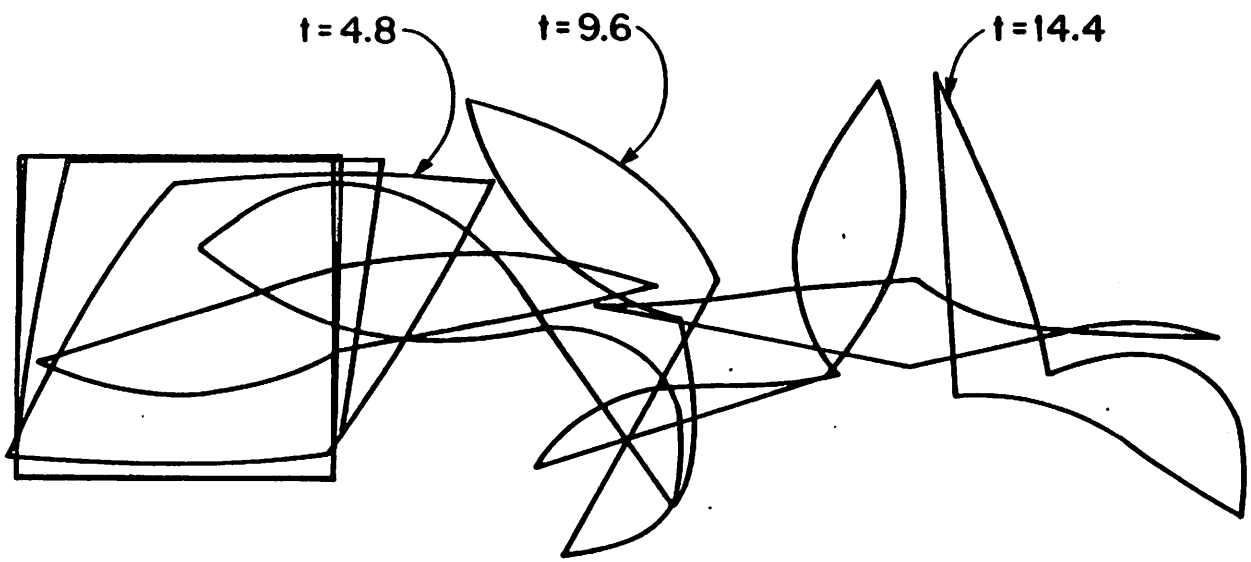

Figure 5.1b. ***Flying closed-loop chain.*** Entire sequence of motion.

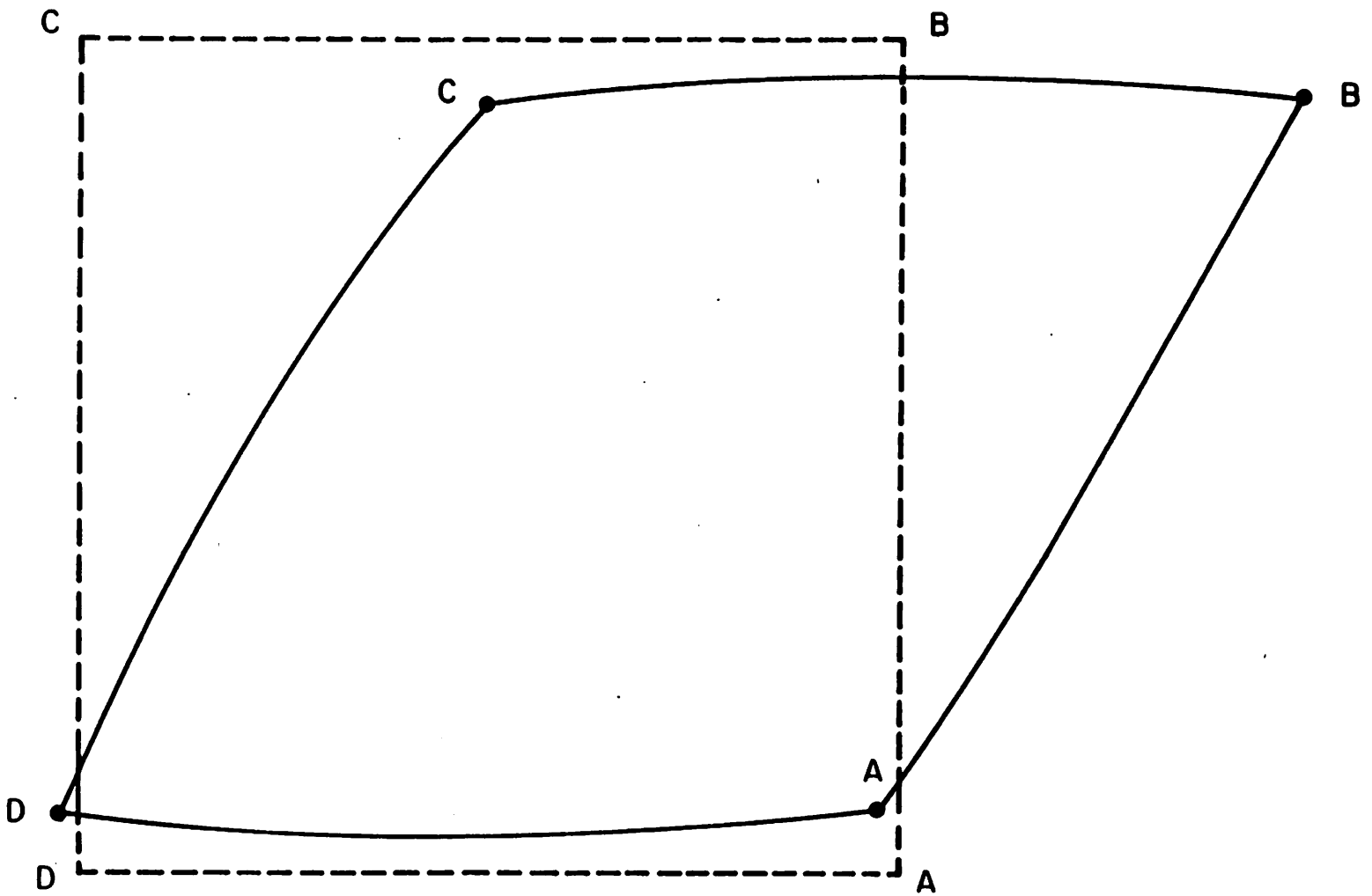

Figure 5.1c. *Flying closed-loop chain.* Deformed shape at time $t = 4.8$.

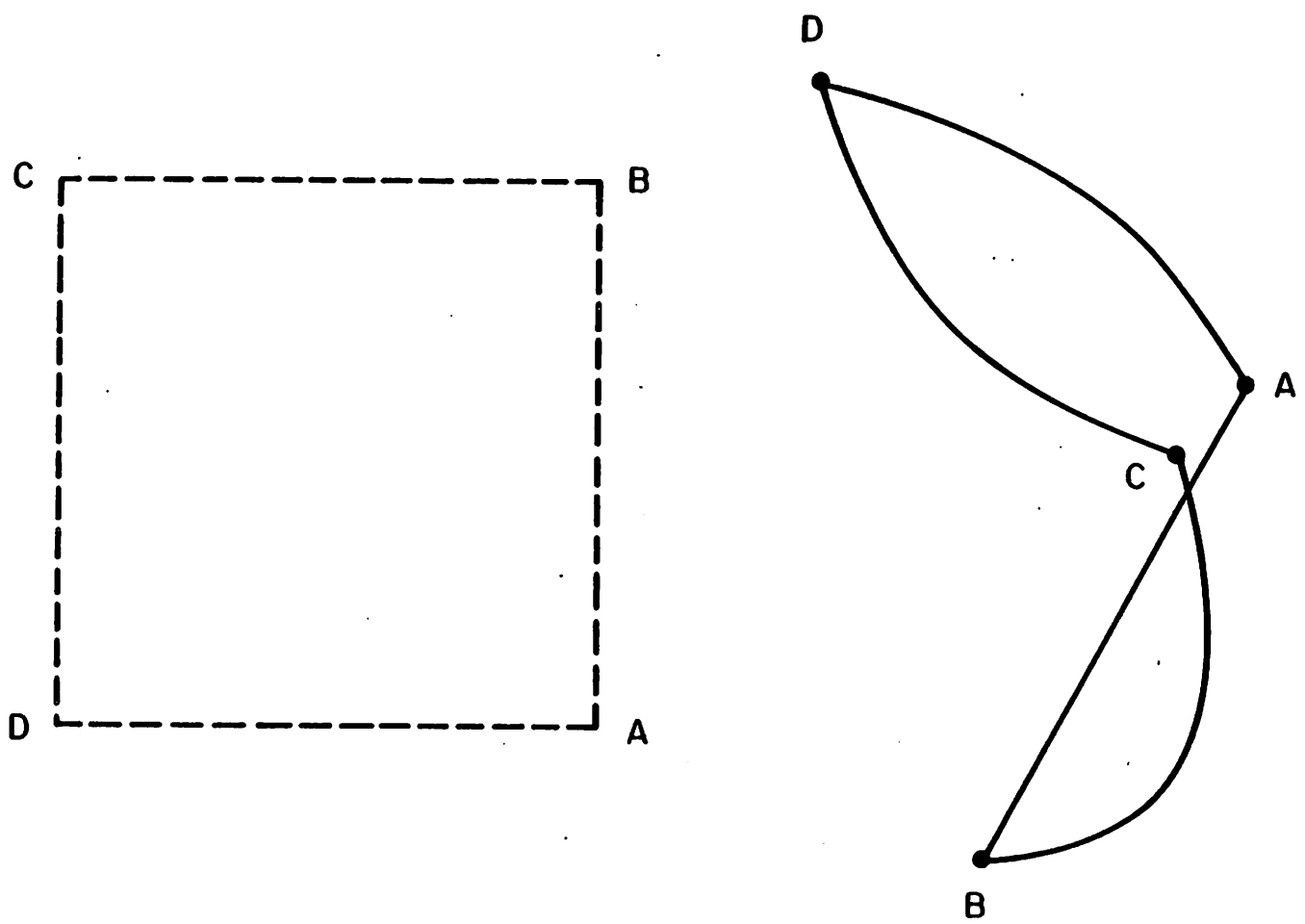

Figure 5.1d. *Flying closed-loop chain.* Deformed shape at time $t = 9.6$.

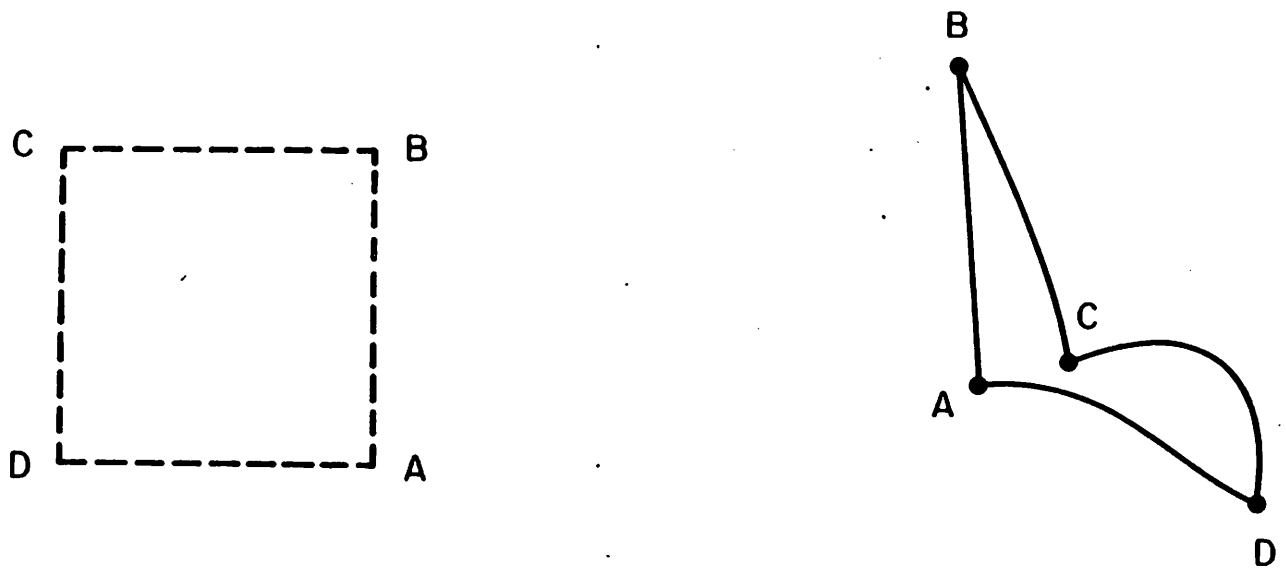

Figure 5.1e. *Flying closed-loop chain.* Deformed shape at time $t = 14.4$.

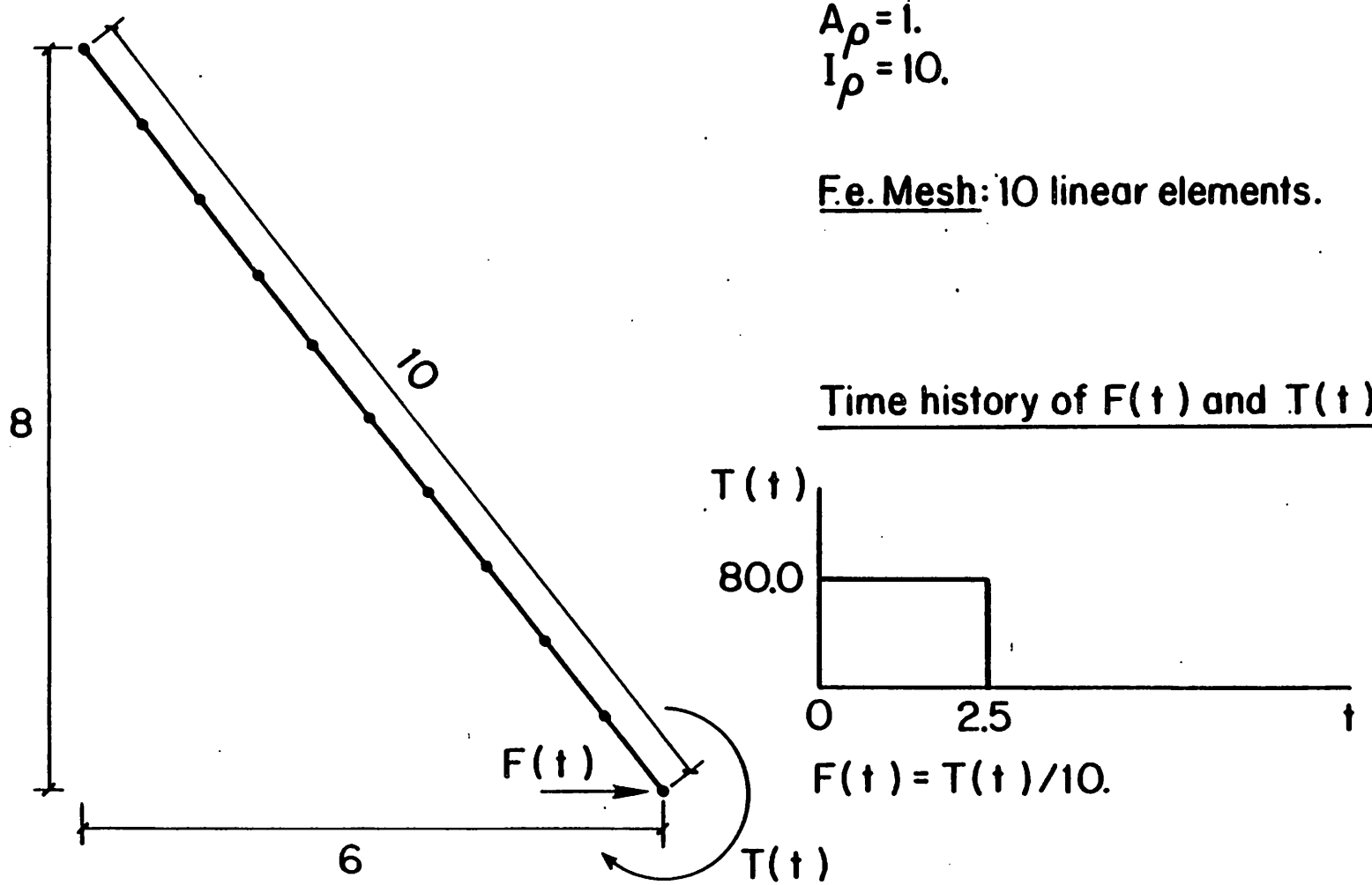

Figure 5.2a. *Flying flexible beam in 3-D motion.* Problem data.

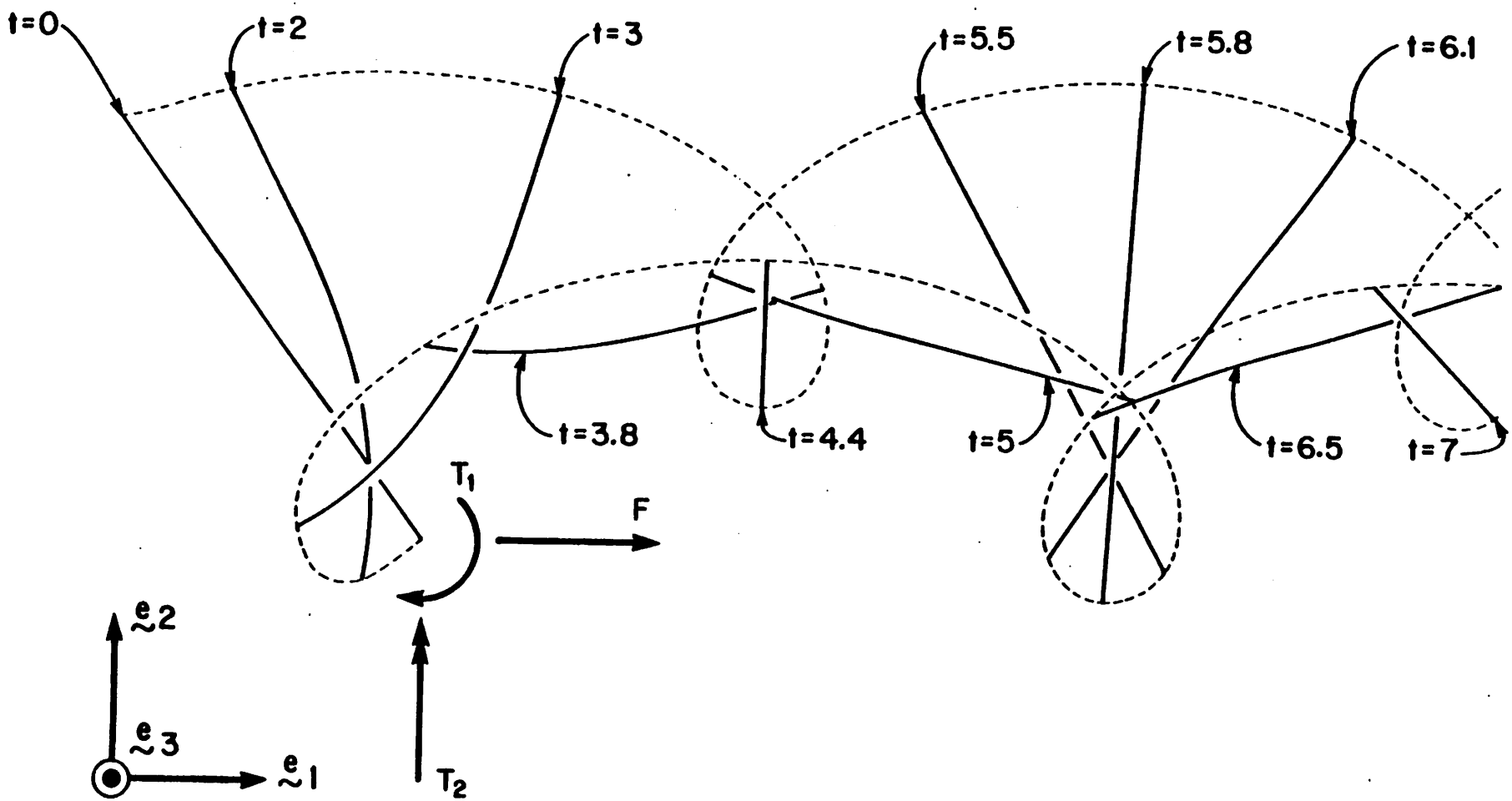

Figure 5.2b. *Flying flexible beam in 3-D motion.* Early tumbling stage.

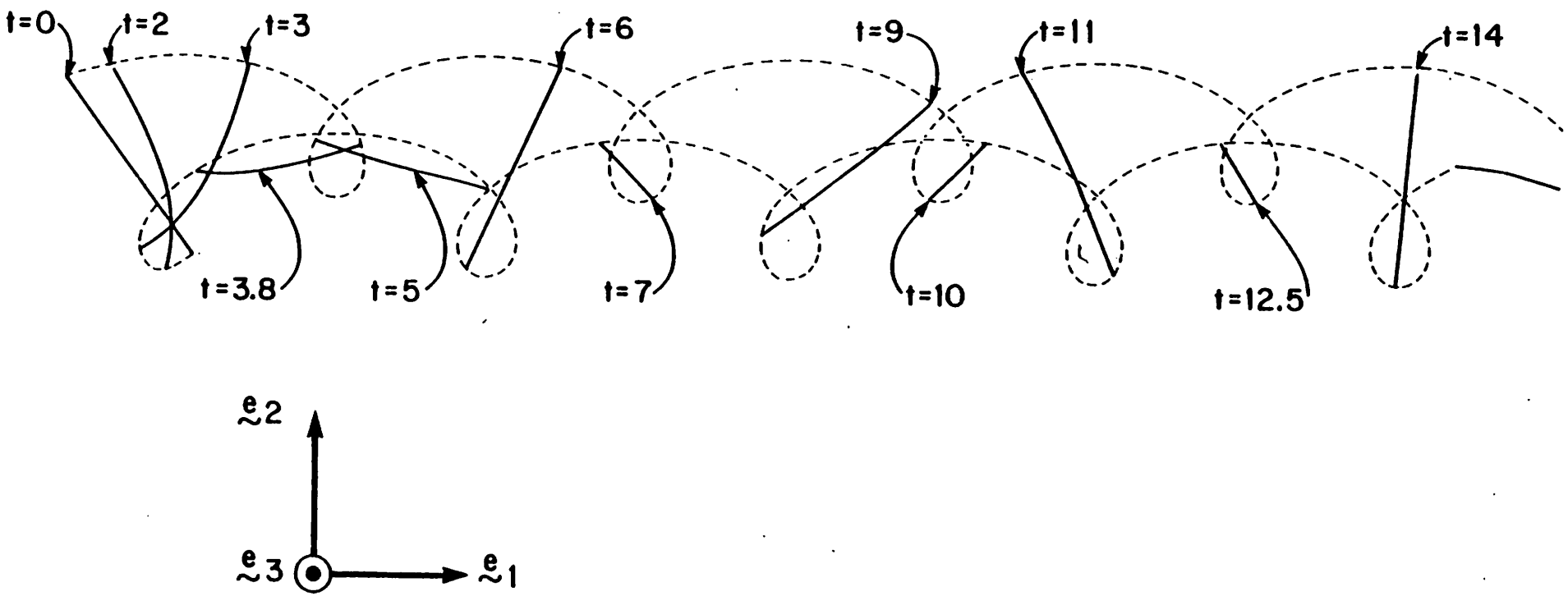

Figure 5.2c. *Flying flexible beam in 3-D motion.* Entire sequence of motion projected on plane ($\mathbf{e}_1$, $\mathbf{e}_2$).

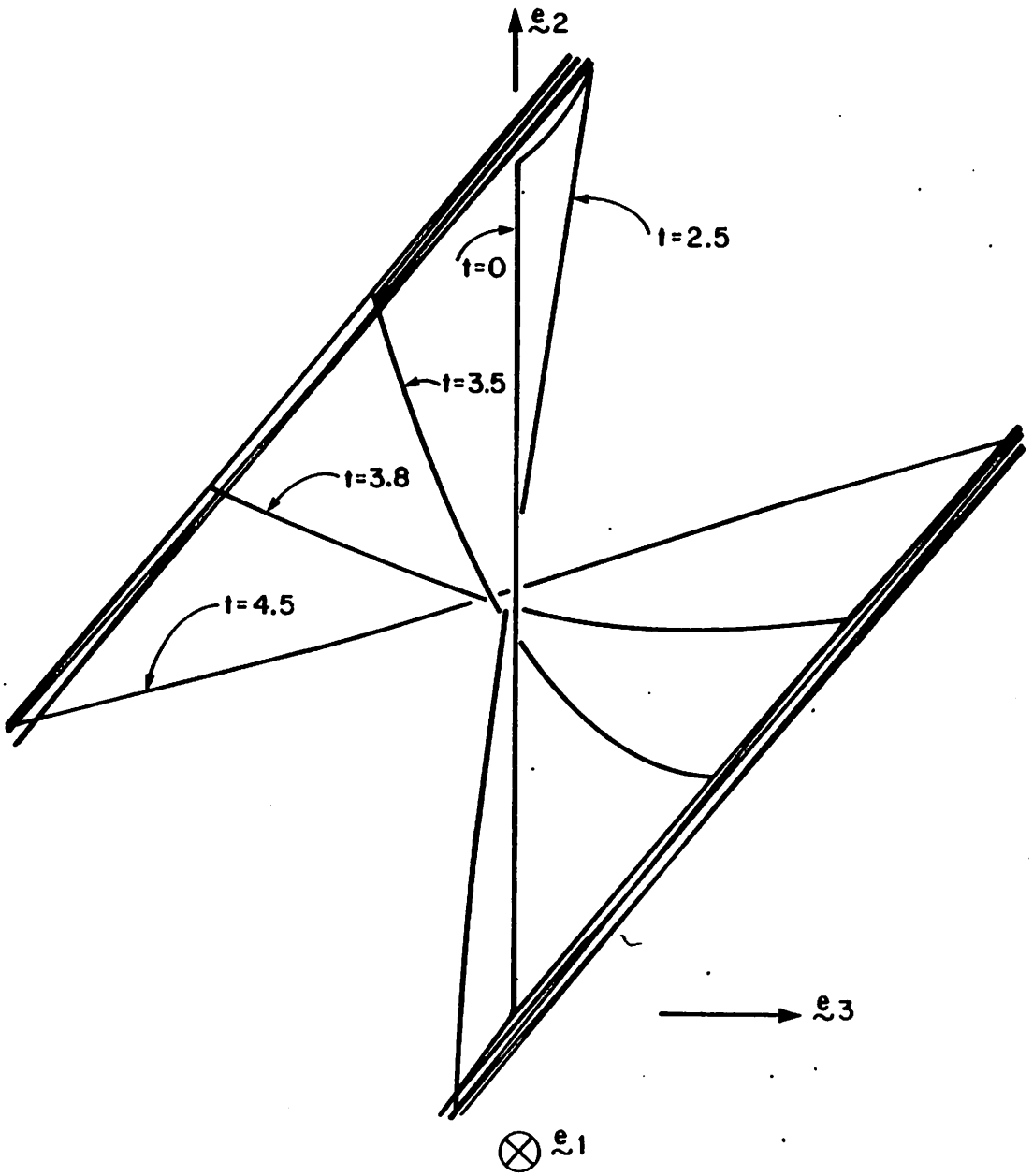

Figure 5.2d. *Flying flexible beam in 3-D motion.* Entire sequence of motion projected on plane ($\mathbf{e}_2$, $\mathbf{e}_3$).

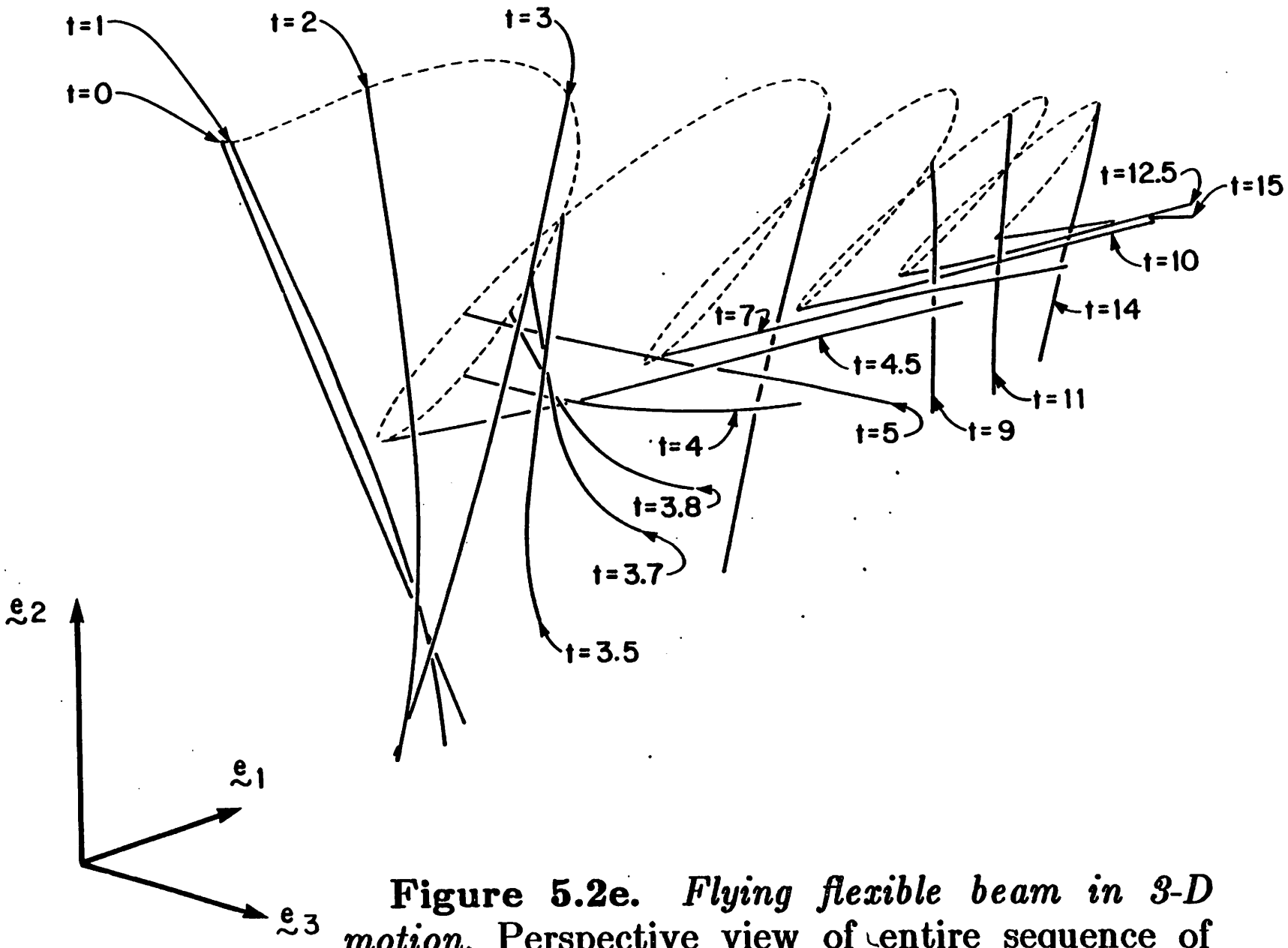

Figure 5.2e. *Flying flexible beam in 3-D motion.* Perspective view of entire sequence of motion from an observer fixed in the inertial frame.

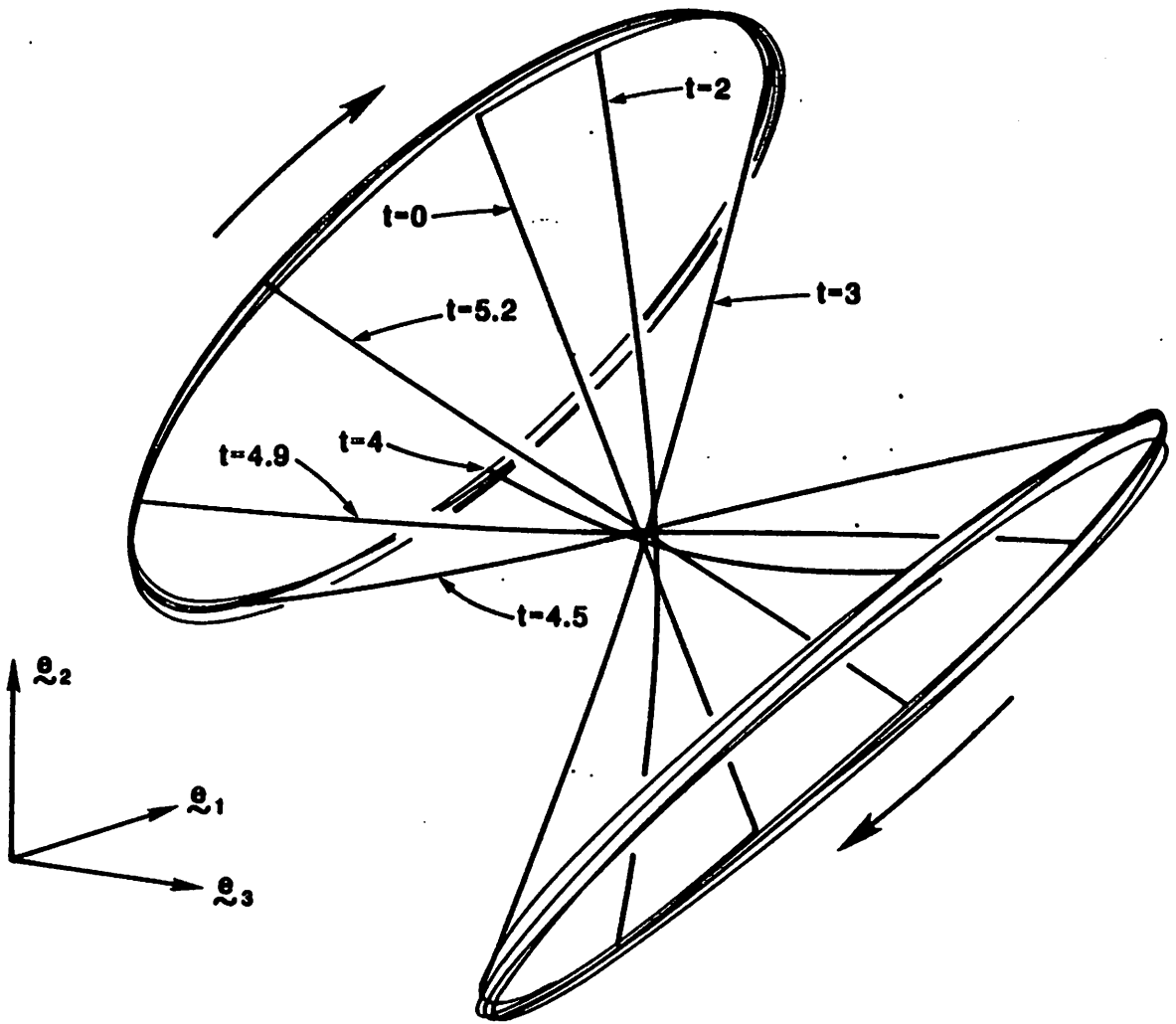

Figure 5.2f. *Flying flexible beam in 3-D motion.* Perspective view of entire sequence of motion, from an observer fixed in the parallel translate of inertial frame.

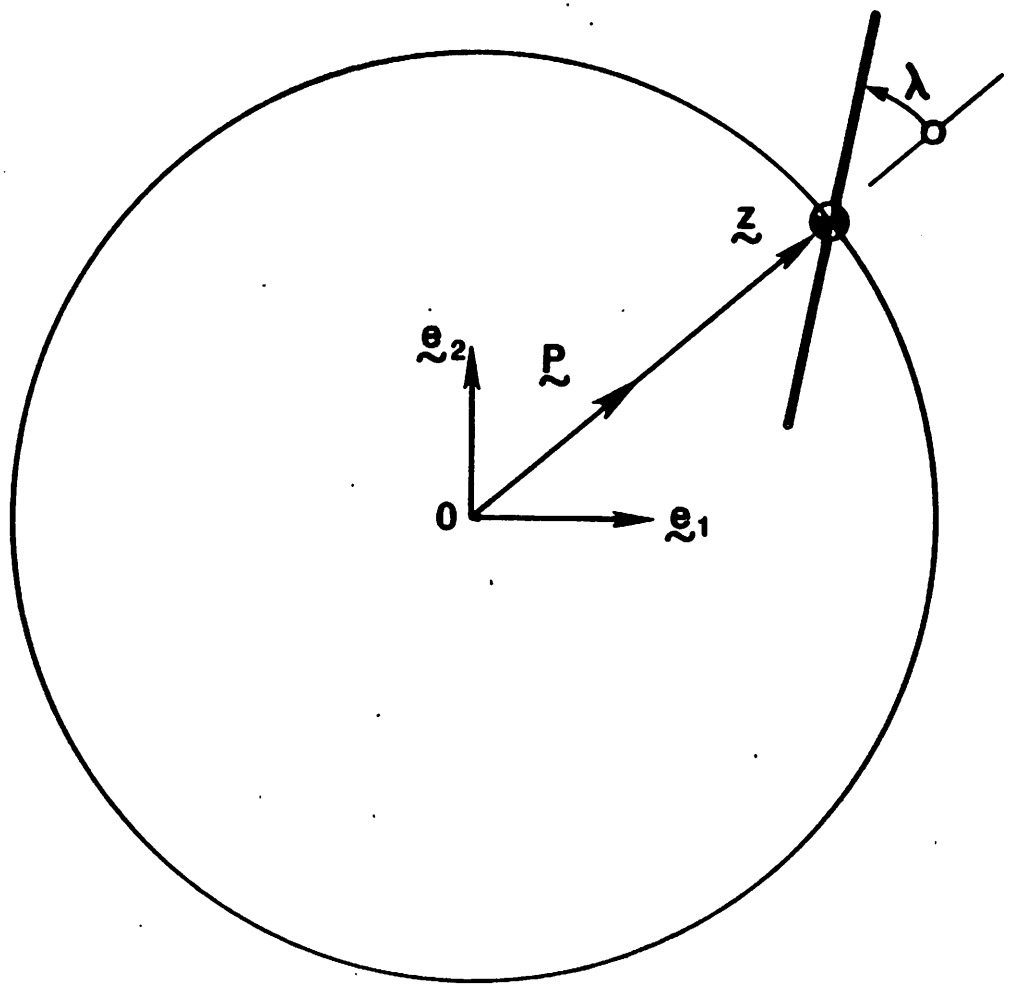

Figure 5.3a. *Satellite dynamics: Libration and orbit transfer.*

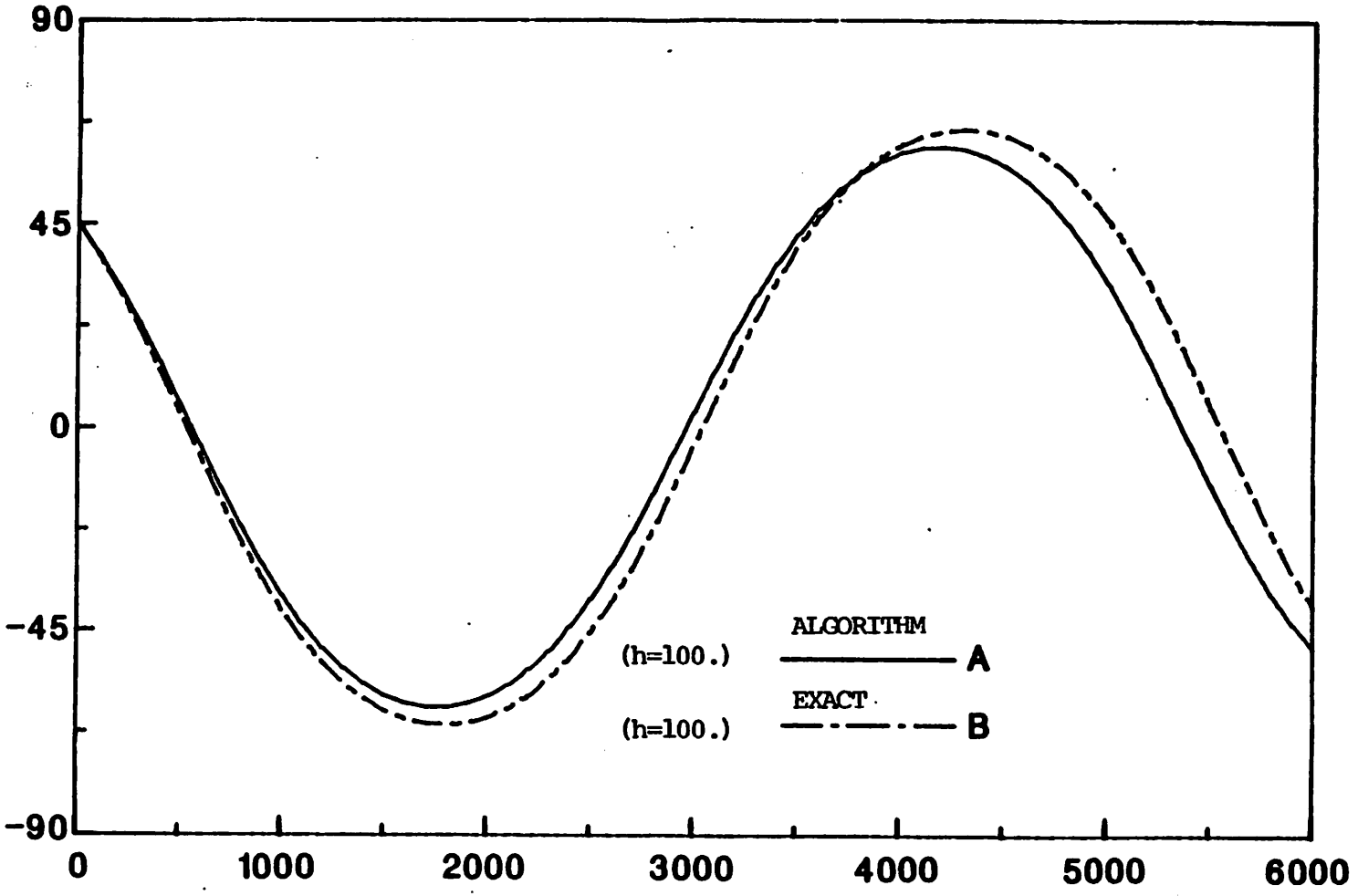

Figure 5.3b. *Satellite dynamics: Libration and orbit transfer.* Evolution of the libration angle λ on lower circular orbit.

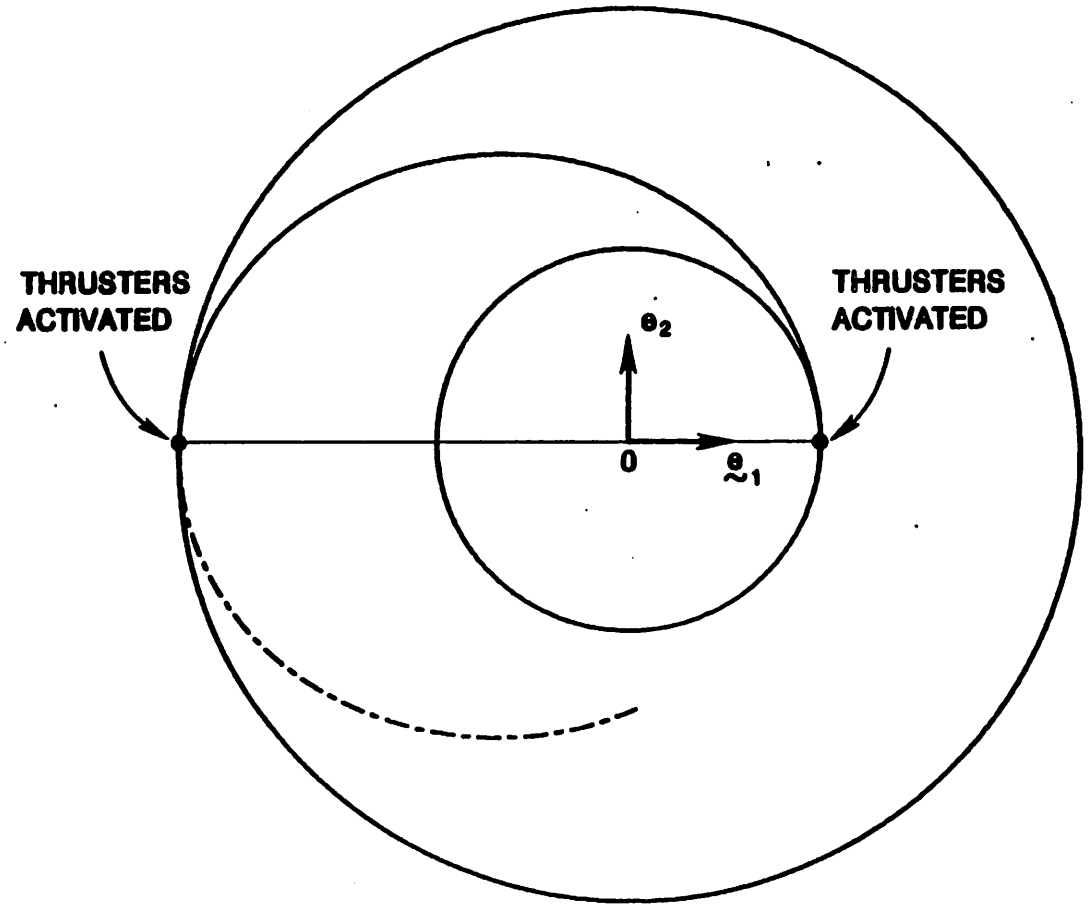

Figure 5.3c. *Satellite dynamics: Libration and orbit transfer.* Transition from lower to higher circular orbits.

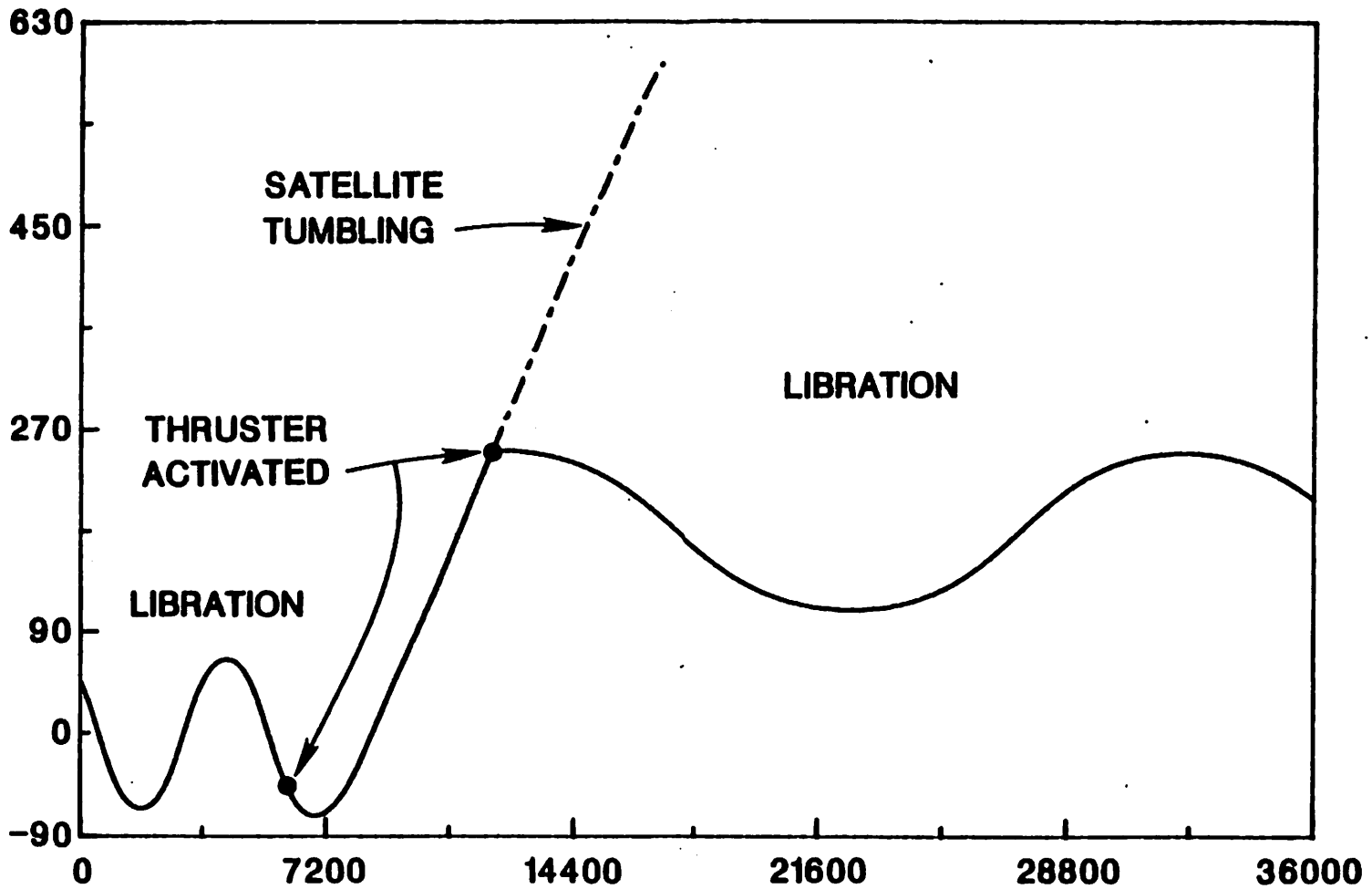

Figure 5.3d. *Satellite dynamics: Libration and orbit transfer.* Complete time history of the libration angle.